Sediments in sea ice drive the Canada Basin surface Mn maximum: insights from an Arctic Mn ocean model

B. Rogalla[1], S. E. Allen[1], M. Colombo[1], P. G. Myers[2], K. J. Orians[1]

[1]Department of Earth, Ocean, and Atmospheric Sciences, University of British Columbia, Vancouver, British Columbia V6T1Z4, Canada

[2]Department of Earth and Atmospheric Sciences, University of Alberta, 1-26 ESB, Edmonton, Alberta T6G2E3, Canada

Key Points:

- We developed an ocean model of Mn in the Canadian Arctic Archipelago and the Canada Basin that captures observed spatial variations
- Non-local sediments transported by sea ice are a key source of nutrients such as Mn to the Canada Basin
- Rivers are not as important for Mn on basin scales as generally identified

Corresponding author: Birgit Rogalla, `brogalla@eoas.ubc.ca`

Abstract

Biogeochemical cycles in the Arctic Ocean are sensitive to the transport of materials from continental shelves into central basins by sea ice. However, it is difficult to assess the net effect of this supply mechanism due to the spatial heterogeneity in sea ice content. Manganese (Mn) is a micronutrient and tracer which integrates source fluctuations in space and time. The Arctic Ocean surface Mn maximum is attributed to freshwater, but studies struggle to distinguish sea ice and river contributions. Informed by observations from 2015 Canadian GEOTRACES cruises, we developed a three-dimensional dissolved Mn model within a 1/12 degree coupled ocean-ice model centered on the Canada Basin and the Canadian Arctic Archipelago (CAA). Simulations from 2002 to 2019 indicate that annually, 82% of Mn contributed to the Canada Basin upper ocean is released by sea ice, while rivers, although locally significant, contribute only 4%. Downstream, sea ice provides 18% of Mn transported from Parry Channel into Baffin Bay and rivers supply 4%. While rivers are often considered the main source of Mn, our findings suggest that in the Canada Basin they are much less important than sea ice. However, within the shelf-dominated CAA, both rivers and sediment resuspension are important. Climate induced disruption of the transpolar drift may reduce the Canada Basin Mn maximum and supply downstream. Other nutrients found in sediments, such as Fe, may be similarly affected. These results highlight the vulnerability of the biogeochemical supply mechanisms in the Arctic Ocean and the subpolar seas to climatic changes.

Plain Language Summary

Autumn storms on the Siberian side of the Arctic Ocean churn up sediment that freezes into sea ice. The prevailing ocean currents and winds push this sea ice across the Arctic Ocean towards the Canada Basin, where it melts and releases the sediment into the ocean. Sediment contains manganese (Mn) and other nutrients that help support plankton and life. Using our Mn ocean model, 82% of Mn in the Canada Basin comes from "dirty" sea ice from 2002 to 2019, while rivers supply 4%. As a result of climate change, less dirty sea ice may make it across the Arctic Ocean, which could reduce this supply system of Mn and other similar nutrients. This also has impacts downstream: water from the Canada Basin travels through the shallow Canadian Arctic Archipelago (CAA) into Baffin Bay and eventually the North Atlantic. We found that about 18% of Mn transported along this route comes from "dirty" sea ice. In the CAA, other sources contribute

as well: tides churn up sediments from the ocean floor and many rivers flow into the channels. Our study highlights ways in which climate change may impact the nutrient supply systems in the Arctic Ocean.

1 Introduction

As the sea ice regime in the Arctic Ocean transitions from multi-year ice to predominantly first-year ice with overall reductions in sea ice extent, thickness and altered drift patterns (Stroeve et al., 2012; Stroeve & Notz, 2018; Spreen et al., 2011; Kwok et al., 2013), biogeochemical cycles and primary productivity are impacted through changes to the sea ice supply mechanism. The Arctic Ocean continental shelves in particular, connect land and ocean through the transfer of river runoff and sea ice from near-shore regions to the central basins (Charette et al., 2016). Reductions in sea ice export from the shelves weaken the long range transport of ice-rafted matter (Krumpen et al., 2019), including sediments (Dethleff et al., 2000; Darby et al., 2011), nutrients and trace metals (Tovar-Sánchez et al., 2010; Measures, 1999), pollutants (Pfirman et al., 1995; Peeken et al., 2018) and climate-relevant gases (Damm et al., 2018), to the surface ocean in regions far away from boundary sources. It is challenging to quantify the contribution of materials supplied by sea ice with observations alone due to the high spatial and temporal variability in the amount of sediment in sea ice and because it is difficult to distinguish from additional contributions to the surface ocean such as river runoff. However, it is clear that changes to the physical processes in the Arctic Ocean will have impacts on the biogeochemical cycles and primary productivity of the basins themselves, as well as downstream in subpolar seas (Drinkwater & Harding, 2001; Greene & Pershing, 2007).

Continental shelves cover half of the area of the Arctic Ocean (Jakobsson, 2002) and their shallow depths facilitate the incorporation of suspended matter into sea ice as it forms (Kempema et al., 1989). The narrow and deeper North American shelves are not as important for basin-wide sea ice sediment transport as the wide Siberian shelves (Eicken et al., 2005). In the Siberian shelf regions, fast ice builds up near shore in the fall, coinciding with storm-related resuspension events, forming sediment-rich sea ice (Nürnberg et al., 1994). The transpolar drift transports this sea ice towards the North Pole and the anticyclonic Beaufort Gyre redirects a portion into the Canada Basin. This passage takes several years, during which the ice undergoes cycles of melting, freezing and deformation. The materials released by melt alter the geochemical signature of the underlying water (Pfirman et al., 1995). While several studies indicate an increase in exchange of ice-rafted material through increased drift speeds (Spreen et al., 2011; Newton et al., 2017), a recent study indicates a disruption of the long range transport of sediments by sea ice due to the melt of first-year ice before it is incorporated into the transpolar drift (Krumpen et al., 2019) with implications for the surface ocean of the endmembers of this transport pathway: Fram Strait, and indirectly the Canada Basin, the Canadian Arctic Archipelago, and the subpolar North Atlantic. In order to establish the importance of sediment from sea ice for biogeochemical cycles in the indirectly impacted regions of the Canada Basin and the Canadian Arctic Archipelago, we developed a model of dissolved manganese (Mn).

Mn is reactive trace element and an important micronutrient which shares many sources with iron (Fe) in the Arctic Ocean (Brand et al., 1983; Bruland et al., 1991; Jensen et al., 2020). Mn has a scavenged-type profile with high concentrations near sources and low background concentrations. This contrast makes it a convenient source tracer. Over the Arctic Ocean shelves, sediment resuspension contributes Mn to the lower water column (Evans & Nishioka, 2018; Colombo et al., 2020). However, the majority of external sources supply Mn to the ocean surface, contributing to the surface Mn maximum. In the Arctic Ocean, this surface maximum is attributed to freshwater sources (Campbell & Yeats, 1982; Yeats & Westerlund, 1991; Middag et al., 2011b; Cid et al., 2012; Kondo et al., 2016; Colombo et al., 2020). Observational studies have identified the origin of this freshwater as river discharge (Campbell & Yeats, 1982; Yeats & Westerlund, 1991; Evans & Nishioka, 2018), sea ice meltwater (Measures, 1999; S. Wang et al., 2014) (for Fe), or a combination of both (Middag et al., 2011b; Cid et al., 2012; Kondo et al., 2016; Colombo et al., 2020). Observations of riverine Mn indicate significantly higher concentrations than in the ocean (Colombo et al., 2019). Similarly, trace metals and nutrients in sea ice occur in concentrations in excess of those in the ocean (Campbell & Yeats, 1982; Hölemann et al., 1999; Granskog et al., 2003; Krachler et al., 2005; Aguilar-Islas et al., 2008; Tovar-Sánchez et al., 2010; Kondo et al., 2016; Evans & Nishioka, 2018). The importance of these components depends in part on the distance and pathway of input into the ocean (Fichot et al., 2013). So, while the Canada Basin is relatively distant from land, the narrow and shallow systems of channels that make up the CAA are in close contact with the land-ocean interface and may be more directly impacted by boundary processes such as river discharge and sedimentary inputs.

In order to distinguish the individual importance of external Mn sources within the Canada Basin and the CAA, model studies are needed. Past studies have used tracers such as terrestrial dissolved organic matter (Fichot et al., 2013) and the oxygen isotope ratio (Yamamoto-Kawai et al., 2009) to distinguish the contributors to freshwater in the Canada Basin. Mn is an interesting complementary tracer because of its role as a nutrient and because it integrates processes that fluctuate on a short time scale. As a result, Mn helps address one of the main limitations of the study of sediment entrainment and export events by sea ice: that they are episodic and localized in nature (Eicken et al., 2005). Similarly, while sediment resuspension occurs intermittently, Mn integrates the effect of this component on the lower water column. After establishing the contributions of the Mn sources, we use Mn as a tool to study the general role of sea ice transport for biogeochemical cycles.

In this paper, we present a model of Mn in the Canadian Arctic Archipelago and the Canada Basin, informed by in situ observations collected during the 2015 Canadian GEOTRACES cruises (Colombo et al., 2020). Our work builds on the comprehensive first global model of Mn in the ocean (Van Hulten et al., 2017) and previous smaller scale models of Mn in the North Pacific Ocean (Johnson et al., 1996) and near hydrothermal vents (Lavelle et al., 1992). We incorporate new parameterizations for sediment resuspension, release of shelf sediments in sea ice, and fluvial contributions, to capture the drivers of Mn distributions in the Canadian Arctic. With this model, we show that the long range transport of sediments by sea ice from the Siberian shelves drives the surface Mn maximum in the Canada Basin while riverine contributions, although locally significant, are not as important as generally identified. Using these results, we discuss implications of future sea ice melt on Mn and Fe nutrient budgets in the Canada Basin and downstream in the Canadian Arctic Archipelago and Baffin Bay.

2 Methods

2.1 Coupled Ocean-Ice Model

For our simulations, we use ocean and ice dynamics calculated by the Arctic and Northern Hemispheric Atlantic (ANHA12) configuration (Hu et al., 2018) of the Nucleus for European Modelling of the Ocean (NEMO) version 3.4 (Madec, 2008). The ANHA12 configuration has a nominal horizontal resolution of 1/12° which resolves freshwater fluxes associated with coastal currents in the CAA, as well as eddies (Bacon et al., 2014; Chelton et al., 1998). The position of the grid's artificial pole in Northern Canada increases the resolution in the CAA to about 2-3 km (Fig. 1). In the vertical, there are 50 depth levels ranging from 1 m thickness at the surface to 454 m near the bottom. The bottom bathymetry is represented using partial steps.

The ANHA12 domain has two open boundaries: one in Bering Strait and the other at 20°S in the Atlantic Ocean. These boundaries are forced with Global Ocean Reanalyses and Simulations data (Masina et al., 2017). The ocean surface is forced with hourly atmospheric data from the Canadian Meteorological Centre's global deterministic prediction system (Smith et al., 2014) and the rivers are forced with monthly runoff climatology with enhanced Greenland melt runoff (Dai et al., 2009; Bamber et al., 2012). The river forcing from 2010 is repeated for the following years (Hu et al., 2019).

The sea ice in ANHA12 is represented using the dynamic and thermodynamic Louvain-la-Neuve (LIM2) sea ice model with an elastic-viscous-plastic ice rheology (Fichefet & Maqueda, 1997; Bouillon et al., 2009). An evaluation of LIM2 in the ANHA12 configuration is provided by Hu et al. (2018). The general spatial distribution of ice thickness within the Archipelago is captured well. In the model, the northern CAA has very thick sea ice (> 4 m), the central parts have intermediate thickness ice (2.5-3 m), and there is thin (< 2 m) sea ice on the east side of the CAA and in southern channels. The ANHA12 simulations are limited by the lack of a land-fast ice parameterization, resulting in ice velocities that are higher than observed in Parry Channel, impacting the winter transport (Grivault et al., 2018). In addition, tides are not included and as a result, the polynyas which form due to tidally enhanced mixing are not well reproduced (Hughes et al., 2018).

The advection and diffusion of tracers are calculated within NEMO by the TOP engine (Gent et al., 1995; Lévy et al., 2001). We use the Flow Relaxation Scheme (FRS) for the tracer boundary conditions and tracer advection is calculated with the Total Variance Dissipation (TVD) scheme (Zalesak, 1979). The vertical diffusion of tracers is calculated from the Turbulent Kinetic Energy closure scheme within ANHA12 and the horizontal eddy diffusivity parameter is set to 50.0 $m^2\ s^{-1}$.

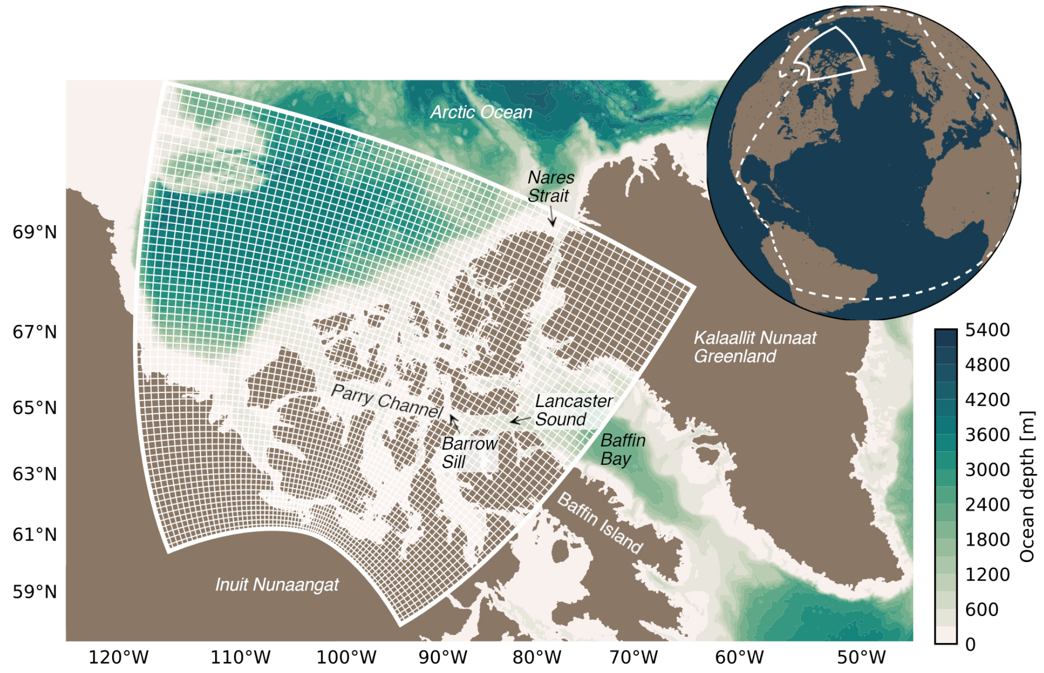

Figure 1. The Mn model domain is centered on the Canadian Arctic Archipelago with highest horizontal resolution in the south (about 3 km). The nominal horizontal resolution of the grid is 1/12°; the white lines depict one in every ten grid points. The solid white line in the inset globe shows the Mn model domain extent, while the dashed white line delineates the domain of the Arctic and Northern Hemispheric Atlantic configuration (Hu et al., 2018) of the ocean-ice model.

2.2 Model of Mn in the Canadian Arctic

The Mn model runs offline in NEMO version 3.6 using five day averaged dynamics fields from the ANHA12 reference run from January 2002 to December 2019 (Hu et al., 2018). The Mn model consists of two main sets of computations: the advection and diffusion of tracers calculated by the NEMO-TOP engine (Gent et al., 1995; Lévy et al., 2001), and the source and sink contributions. The source and sink parameterizations were developed guided by observations from the 2015 Canadian GEOTRACES cruises (Colombo et al., 2020) and inspired by the first global model of Mn (Van Hulten et al., 2017). In order to reduce the computational cost, we calculate the model on a sub-domain of ANHA12, centered on the CAA (Fig. 1). Note that since we are running offline, the physics originates from the full domain.

The known sources and sinks of Mn in the ocean are: rivers, hydrothermal vents, sediment diffusion, sediment resuspension, reversible scavenging, sinking, uptake and remineralization, atmospheric dust deposition, and flux from ice (Middag et al., 2011b; Balzer, 1982; Klinkhammer & Bender, 1980; Evans & Nishioka, 2018). From this list, we incorporate the processes that are important for dissolved Mn in the Arctic (summarized in Fig. 2 and Eqn. 1 and 2). In order to model the reversible scavenging of Mn, we incorporate Mn oxides (oMn) in addition to dissolved Mn (similar to Van Hulten et al. (2017)). We do not model particle-bound Mn (pMn), but rather incorporate the indirect effect of pMn onto dMn through dissolution from the source components. We did not incorporate hydrothermal vents as a source of Mn in the Arctic, since the influence of the Gakkel Ridge is restricted to Nansen and Amundsen Basins due to scavenging nearby the source (Lavelle et al., 1992; Middag et al., 2011b). We also do not include sediment diffusion (reductive dissolution) nor biological uptake and remineralization because observations have indicated that these processes are not significant for Mn in the CAA (Colombo et al., 2020). The overall Mn model equations are:

$$\frac{\partial dMn}{\partial t} = S_{river} + S_{sediment} + S_{atm} + S_{ice} + S_{sed\ ice} + R_{scav} + advection + diffusion \quad (1)$$

$$\frac{\partial oMn}{\partial t} = -R_{scav} - R_{sink} + advection + diffusion \quad (2)$$

which includes the contribution of rivers, S_{river}, sediment resuspension (non-reductive dissolution), $S_{sediment}$, atmospheric dust deposition, S_{atm}, dust flux from ice, S_{ice}, sediment released by ice, $S_{sed\ ice}$, and the reversible scavenging terms, R_{scav}. The details of the parameterizations are described in the following sections and the parameter values used for the base run are listed in Table 1.

The model was initialized with output from the global Mn model (Van Hulten et al., 2017) and at the sub-domain boundaries, concentrations are held constant. At the model boundaries, the ratio of dissolved to oxidised Mn from the global model were not representative (oxidised Mn was too low) and resulted in unusual scavenging behavior. To address this, we took values for the dissolved and oxidised Mn concentrations in a band 15 grid cells towards the interior of the basin (where the model had established normal scavenging behavior) from a test model run at the end of spin up and used those values for the boundary conditions.

Table 1. Constants and parameter values used in the Mn model runs.

Parameter	Description	Value	Source
α_0	Solubility of Mn at 4°C	0.65	Fishwick et al. (2018)
$f_{Mn\ crust}$	Mn fraction in Earth's crust	527 ppm	Wedepohl (1995)
$f_{Mn\ sed}$	Mn fraction in marine sediment	270 ppm	Macdonald and Gobeil (2012)
m	Molar mass of Mn	54.938 g mol^{-1}	—
k_d	Reduction and desorption rate	$4.72 \cdot 10^{-7}$ s^{-1}	Bruland et al. (1994)
	Photoreduction rate	$2.72 \cdot 10^{-5}$ s^{-1}	Sunda and Huntsman (1994)
k_p	Oxidation and adsorption rate	$7.00 \cdot 10^{-7}$ s^{-1}	This study[a]
s_{ox}	Sinking rate	1-10 m day^{-1}	Van Hulten et al. (2017)
C	Tidal erosion tuning constant	$3.3 \cdot 10^{-6}$	This study
γ	Solubility tuning constant	0.065	This study
R / SPM	River characteristic content		This study[b]
	- Glacial	164 nM / 261 mg L^{-1}	
	- Continental	30 nM / 12 mg L^{-1}	
	- Other	5 nM / 4 mg L^{-1}	

[a]Using data from Colombo et al. (2020); Li (2017).

[b]Using data from Colombo et al. (2019); Brown et al. (2020).

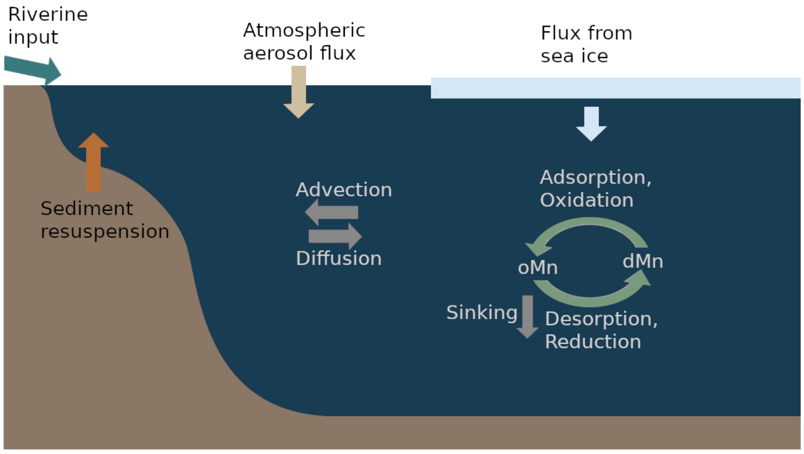

Figure 2. Summary of the processes that affect Mn concentrations in the Canadian Arctic Archipelago and the Canada Basin.

2.2.1 Riverine Source

River discharge contributes Mn to the shelf seas and into the Arctic Ocean (Middag et al., 2011a). Dissolved Mn is contributed directly in its dissolved form and indirectly through the dissolution from particle-bound Mn. The contribution of riverine Mn depends on the river discharge, Q, and the concentration in the rivers. These concentrations vary based on properties of the river's catchment basin: glacial rivers are strongly enriched in dissolved Mn, continental rivers are somewhat enriched, and in all other rivers, Mn is not significantly enriched (Colombo et al., 2019). At each time step, the rivers contribute dissolved Mn following:

$$S_{river} = \overbrace{\frac{Q}{\rho_0\ \Delta z_{surface}} R_{class}}^{dissolved\ Mn} + \beta \overbrace{\frac{Q}{\rho_0\ \Delta z_{surface}} \frac{SPM_{class} \cdot f_{Mn,\ crust} \cdot \alpha_0}{m}}^{particle\ origin\ dissolved\ Mn} \tag{3}$$

where ρ_0 is the density of the river water, $f_{Mn,\ crust}$ is the crustal abundance of Mn, α_0 is the solubility of Mn, m is the molar mass of Mn, $\Delta z_{surface}$ is the surface grid box thickness, and β is a factor which ranges from 0-1 in our experiments. We use an average value of the solubility of Mn (65%) measured in seawater at 4°C, since this lower temperature better reflects the CAA (Fishwick et al., 2018). This solubility falls within the range measured in samples across the world (Fishwick et al., 2018). Each river is assigned a class with an associated characteristic trace metal concentration, R_{class}, and suspended particulate matter content, SPM_{class}, based on catchment basin properties: glacial, con-

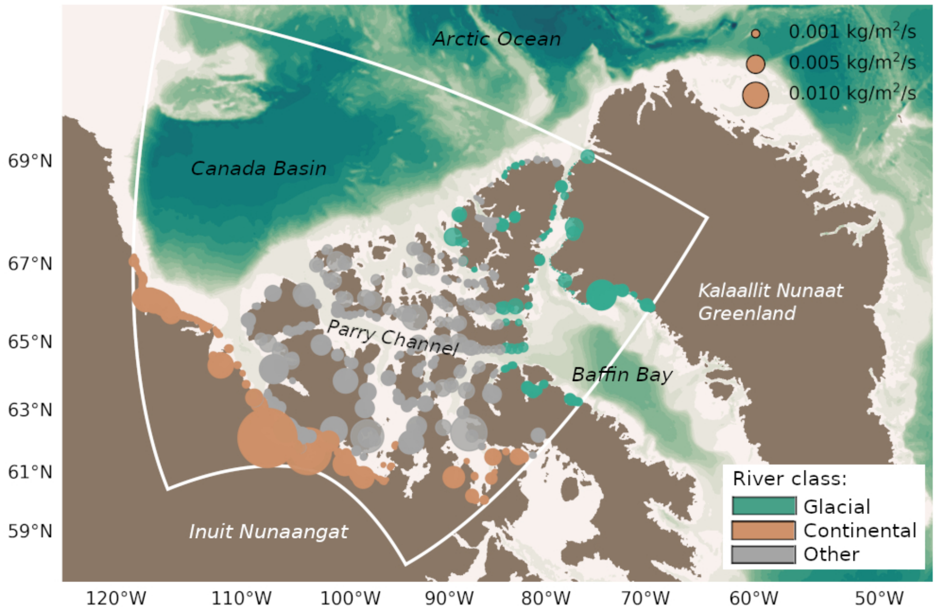

Figure 3. Model rivers were classified based on their drainage basin properties: glacial (green), continental (orange), or other (gray). The points in this map are the locations of the river mouths in the model and their sizes are proportional to the river discharge in September, 2015 (forcing is repeated from year 2010). Note that the river mouths are remapped to accurately represent the ocean freshwater circulation, hence some large rivers are represented as single point sources, while others such as the Mackenzie River consist of multiple point sources along the coastline (Hu et al., 2019; Hayashida et al., 2019).

tinental, and other (Fig. 3). The Mn concentrations and SPM content associated with the classes are determined from rivers sampled in the CAA (Colombo et al., 2019; Brown et al., 2020). In the base case, the Mn concentrations in glacial rivers are 164 nM, continental rivers 30 nM, and all other rivers 5 nM. The SPM content is 261 mg L^{-1} in glacial runoff, 12 mg L^{-1} in continental runoff, and 3 mg L^{-1} in all other rivers.

2.2.2 Atmospheric Aerosol Flux and Release from Sea Ice

Atmospheric aerosols contribute Mn to the ocean through direct deposition to surface waters, Φ_{atm}, or through the deposition onto sea ice and the subsequent release during melt, Φ_{ice}. We parameterized this contribution as:

$$S_{atm\ or\ ice} = \frac{\alpha_0 \cdot f_{Mn\ crust}}{m \cdot \Delta z_{surface}} \cdot \Phi_{atm\ or\ ice} \tag{4}$$

The atmospheric and sea ice flux terms are derived from monthly Community Earth System Model (CESM) results. The combined monthly dry and wet atmospheric deposition fluxes originate from historical (1920-2005) and future (2006-2080) runs of the Community Atmosphere Model with Chemistry (CAM-Chem) downloaded from the Climate Data Gateway (CESM1 CAM5 BGC Large Ensemble Atmosphere Post Processed Data; Tilmes et al. (2016). We estimate tracer fluxes from ice using the monthly Community Ice CodE ensemble results (CICE; Holland et al. (2012); Kay et al. (2015)). These ensemble run sets have a horizontal atmospheric resolution of 0.9 x 2.5° and ocean/ice resolution of 1.6 x 2.5° which we linearly interpolated to the ANHA12 grid.

2.2.3 Sediment Resuspension over the Continental Shelf

Dissolved Mn increases near the ocean floor in the Canadian Arctic as a result of sediment resuspension (Colombo et al., 2020). Sediment resuspension occurs intermittently, however, Mn integrates the resuspension events and thereby provides a cumulative view. We incorporated sediment resuspension as a continuous process:

$$S_{sediment} = \Phi_{erosion} \cdot \frac{\alpha \cdot f_{Mn\ sed}}{m \cdot \Delta z_{bottom}} \tag{5}$$

where $f_{Mn\ sed}$ is the fraction of Mn in marine sediments. The fraction of Mn found in marine sediments is likely to be lower than those measured in the continental crust (i.e. Wedepohl (1995)), since it's undergone some amount of chemical transformation. So, we used the Mn fraction estimated by Macdonald and Gobeil (2012) which is based on sediments in cores on the shelf and slope regions surrounding the Canada Basin. In Eqn. 5, $\Phi_{erosion}$ is the "erosion ability" (see Fig. S7 for the forcing field). This term incorporates the spatial differences in dynamics within the CAA. West of Barrow Sill, the system has lower mixing rates (Hughes et al., 2018) and tidal speeds (Epstein, 2018), than the region east of Barrow Sill and around the central sill area. These differences impact the sediment resuspension rates, apparent in the much stronger near-bottom increases of observed dMn in the eastern CAA (Colombo et al., 2020). We estimate the ability of sediment to be eroded with the barotropic tidal speed, U_{tidal}, and a tuning constant, C:

$$\Phi_{erosion} = C \cdot U_{tidal}^2 \tag{6}$$

The barotropic tidal speeds are from the MOG2D-G model (Carrère & Lyard, 2003) and are significantly higher in the eastern CAA, compared to the western CAA (Epstein, 2018). Locations where the tidal speeds are less than 1 cm s^{-1} are masked, since this is below a critical threshold for motion for particles greater than 0.1 mm (i.e. sand). In areas where resuspension occurs frequently, the easily accessible Mn on particles has already been removed, resulting in a lower solubility. So, we reduce the solubility in Eqn. 5 at high tidal speeds according to:

$$\alpha = \alpha_0 \cdot \frac{\gamma(1 - e^{-U_{tidal}^2/\gamma})}{U_{tidal}^2} \tag{7}$$

where γ is a tuning parameter. At small tidal speeds, Eqn. 7 approaches α_0 while at tidal speeds greater than about 0.14 m s^{-1}, the solubility becomes smaller and as a result, the overall resuspension rate approaches a constant $\alpha_0 \gamma C$ (Fig. S8). The tuning parameters were estimated based on the best fit to mean observations from several tuning runs.

2.2.4 Sediment Entrained in Sea Ice and Subsequent Melt

Sediment entrained in sea ice has been identified as an important source of reactive trace metals such as aluminum and iron in the ocean, and thus may also be important for Mn (Measures, 1999). In order to parameterize this contribution, we couple the Mn contained in sediments in sea ice and the sea ice melt rate, I_{melt}:

$$S_{sed\ ice} = \frac{\alpha_0 \cdot f_{Mn\ sed}}{m \cdot \Delta z_{surface}} \cdot S_p \cdot I_{melt} \tag{8}$$

where S_p is the sediment content in sea ice at each grid point. The sediment content is spatially variable, and depends on the amount of sediment that was incorporated during ice formation on the shelves and on sea ice transport.

Through particle tracking experiments with Ocean Parcels (Lange & van Sebille, 2017), we estimated the contribution of sea ice formed over the Siberian shelves during the stormy fall months (September-December) to the ice in the Canada Basin. We released parcels every month over the course of a year and traced them backwards for three years (the average sea ice age in the Canada Basin and the northwestern CAA based on satellite information). Almost 40% of the sea ice tracks in the northwestern CAA and Canada Basin region originated from the Siberian shelves via the transpolar drift during the fall months, when strong sediment resuspension events coincide with sea ice formation (Fig. 4). The results of the particle tracking experiments were interpolated and smoothed to create a forcing field which incorporates the spatial variation in sediment content in sea ice (Fig. S6). In addition, we assumed a low background value of shelf sediments in sea ice in the Archipelago.

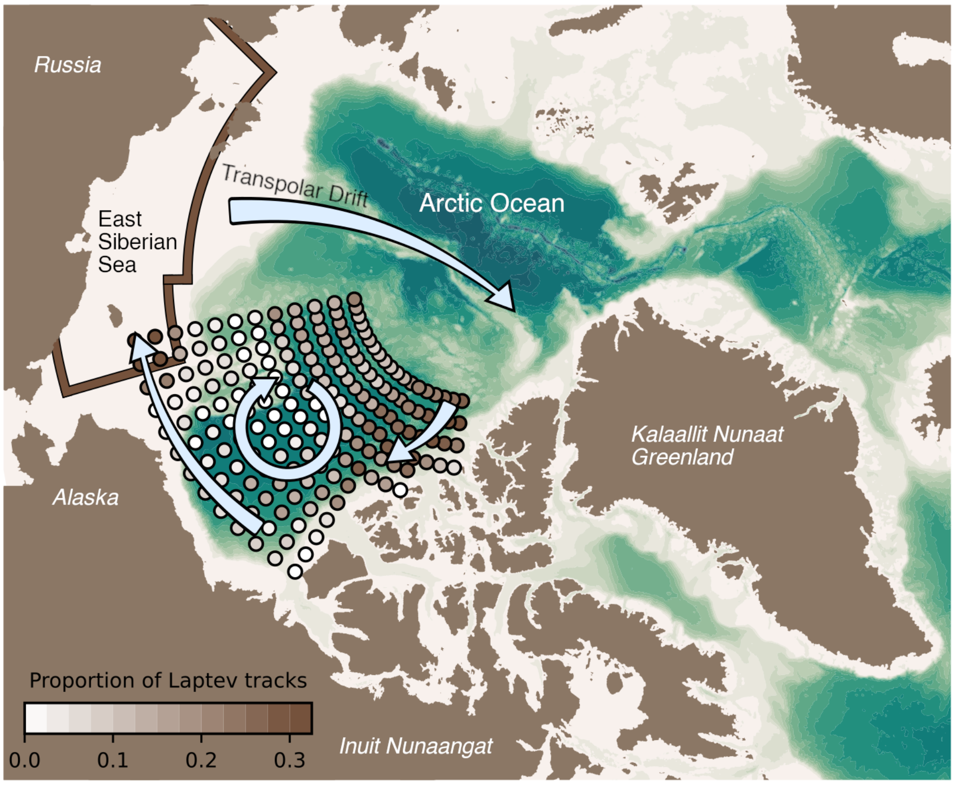

Figure 4. Sediment rich sea ice, produced over the Siberian shelves (East Siberian Sea) in the fall, is transported across the Arctic Ocean via the transpolar drift. From there it is found predominantly along the outer edges of the Beaufort Gyre. As a result, the largest contribution from the Siberian shelves occurs in the northeastern CAA. Ice motion patterns are indicated with light blue arrows. For locations in the Canada Basin, the proportion of parcels traced back to the Siberian shelves (region defined with the brown outline) in the fall months are shown.

2.2.5 Reversible Scavenging and Sinking

Dissolved Mn oxidizes forming larger aggregates and adsorbs to particle surfaces. dMn is regenerated by the reduction of oxidised Mn and desorption from particles. Since we do not directly model particle-bound Mn, but rather incorporate its effect on dMn through dissolution from the source components, we calculate the reversible scavenging based on the dissolved and oxidised Mn concentrations (Van Hulten et al., 2017):

$$R_{scav} = -k_p \cdot [dMn] + k_d \cdot [oMn] \tag{9}$$

where k_p is the adsorption and oxidation rate, and k_d is the desorption and reduction rate (see Text S1 for the full derivation). The R_{scav} term appears with opposing signs in the dMn and oMn equations (Eqn. 1 and 2). We estimate the rate constants from observations of dissolved and particulate Mn in the Canadian Arctic (Li, 2017; Colombo et al., 2020). Assuming steady state, the ratio of the scavenging rates is equal to the ratio of observed dissolved to particulate Mn concentrations. This assumption reduces the available observations to those far away from sources and sinks, i.e. deep stations in Baffin Bay and the Canada Basin (Fig. S1). The ratio of scavenging rates, k_p/k_d, is estimated to be 1.48 and with a k_d of $4.72{\cdot}10^{-7}$ s^{-1} (Bruland et al., 1994), k_p is estimated as $7.00{\cdot}10^{-7}$ s^{-1} (Fig. S2). To account for photoreduction, the reduction rate, k_d, increases from the base rate up to $2.72{\cdot}10^{-5}$ s^{-1} near the surface, proportional to the solar flux that penetrates into the ocean (calculated by ANHA12). The scavenging rates in the model do not depend on the dissolved oxygen concentration since Arctic waters are generally well oxygenated.

The oxidised Mn aggregates sink, R_{sink}, and are removed through burial as in Van Hulten et al. (2017):

$$R_{sink} = s_{ox}\frac{\partial[oMn]}{\partial z} \tag{10}$$

where s_{ox} is the sinking rate.

2.3 Tuning

The model is tuned by altering the sediment content in sea ice and the sediment resuspension rate constant. The resultant sediment content in sea ice in the Canada Basin in our model ranges from 0 to 157 g m^{-3} and the average is 32 g m^{-3}. In observations, the sediment load ranges by several orders of magnitude depending on the location sampled, the type of ice, and is highly variable year-to-year (see Table S1 for a non-comprehensive list of observed sediment content). In the Beaufort Sea, the observed sediment content in ice cores ranged from 31 to 593 g m^{-3} with an average of 157 g m^{-3} (Reimnitz et al., 1993). Our tuned ice sediment content is smaller than observed in that study, but of a similar order of magnitude. The sediment resuspension rates in our model range from 0 to 4425 g m^{-2} yr^{-1} and the average is 149 g m^{-2} yr^{-1}. Particulate material collected in sediment traps over the Beaufort Shelf from spring 1987 to 1988 contained total dry weight particle fluxes ranging from 20 to 140 g m^{-2} yr^{-1} (O'Brien et al., 2006). The largest particle fluxes occurred during the summer and fall. Our average tuned sediment resuspension rate is at the upper end of this range.

2.4 Experimental Design

Three numerical experiments were performed with the Mn model, running from 2002 to 2019: the reference and "clean" sea ice cases, and a sensitivity experiment for the rivers. The reference run includes all model components and uses a lower bound estimate of the river contributions (no particle-bound Mn, $\beta = 0$ in Eqn. 3). The clean sea ice case is the same as the reference run, except that the sea ice does not contain sediment (i.e. $S_{sed\ ice} = 0$). In order to bound the riverine influence, we perform a sensitivity experiment with a distinctly upper bound riverine estimate ($\beta = 1$ in Eqn. 3) and compare this with the reference experiment which provides a lower bound estimate. The treatment of riverine input of Mn introduces uncertainties in the model due to the complex estuarine cycling and the influence of particulate matter on dissolved Mn concentrations. In the "upper bound" river experiment, we include the contribution from riverine sediments on the Mn concentrations in addition to the dissolved Mn. Each experiment is spun up by repeating the year 2002 seven times, before starting the full run. The run is considered spun up when the year-to-year change in Mn profiles is minimal (Fig. S9). Analysis was performed using Python 3 (https://anaconda.com) within Jupyter Notebooks with the NumPy, Pandas, SciPy, Matplotlib, Seaborn, scikit-learn, and cmocean packages (Pedregosa et al., 2011; Hunter, 2007; Kluyver et al., 2016; Oliphant, 2006; The Pandas development team, 2020; Thyng et al., 2016; Virtanen et al., 2020; Waskom & the Seaborn development team, 2020).

3 Results

The Mn profiles throughout our domain are typical for a scavenged type element: concentrations are higher near sources with a low and homogeneous background (Fig. 5). The background concentrations are controlled by scavenging, advection and mixing, and the resultant redistribution of materials throughout the water column, while the surface Mn maximum is a result of the contributions from river runoff, sea ice melt, dust deposition, photoreduction, and sediment that is resuspended directly into the polar mixed layer. Sediment resuspension leads to near-bottom increases in some regions.

3.1 Model Evaluation

We evaluate the Mn model by comparing simulated Mn concentrations from the reference experiment in September 2015 with measurements collected by the Canadian GEOTRACES cruises during the same time period (Colombo et al. (2020); Fig. 5). Our intention was not to replicate the observations, but to incorporate all the processes that control the distribution of Mn and to capture the observed spatial variation. These observations were not used in initial conditions or boundary conditions to allow for an independent evaluation.

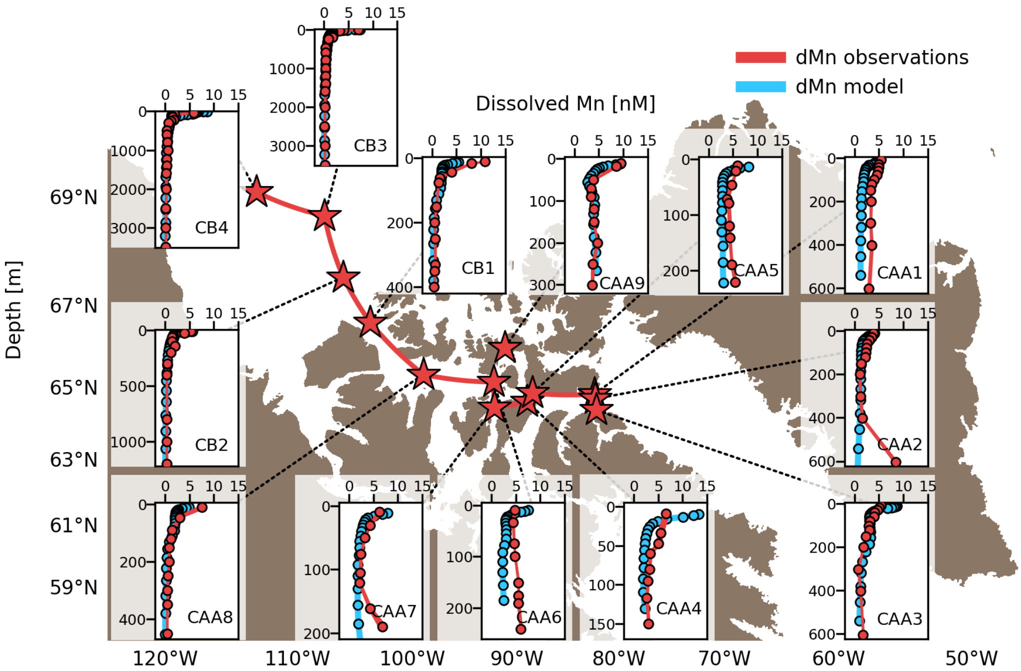

Figure 5. Simulated Mn profiles (blue) from the reference run compared to observed concentrations (red) measured during Canadian GEOTRACES cruises in September, 2015. Station locations are marked by red stars and the station names are labelled on the profiles. The thickness of the red line is the standard deviation of the measurements of the Mn samples.

The modelled Mn concentrations are highest at the surface and low in the background, as in the observations (Fig. 5). The model captures the regional variation of Mn concentrations along a transect from the Canada Basin into the Canadian Arctic Archipelago (Fig. 6). From 0-900 km along this transect (the Canada Basin), background concentrations are low (0-2 nM) and increase in the upper 300 m of the water column to

7-12 nM. At station CB4 in the Canada Basin, both the model and observations indicate high surface concentrations that extend deeper into the water column relative to the rest of the Canada Basin (Fig. 6). Surface concentrations at CB3 are the highest observed in the central part of the Canada Basin. In the model, a band of high concentrations is also found at the surface around station CB3. At 100-200 m depth in the Canada Basin, observed Mn concentrations are slightly higher than the background concentrations. This increase is associated with the winter Bering Sea Water and is not captured by the model. From 1300-2000 km along the transect (the eastern CAA), the background Mn concentrations are higher, ranging from 1-4 nM, due to the prevalence of resuspension and other Mn sources. The increased role of sediment resuspension is particularly noticeable in the near-bottom increase in concentrations in the western CAA (stations CAA4-7; Fig. 6). Surface concentrations at CB1 and CAA8 in the Western CAA are underestimated (Fig. 5) and receive outflow from the Canada Basin. In the eastern CAA, surface concentrations range from 5-10 nM in observations and in the model. However, in the central CAA, surface concentrations are overestimated at stations CAA3-6, mostly at the southern side of Parry Channel and downstream from shallow regions with strong resuspension (Fig. 5). In Lancaster Sound, the model captures the higher surface concentrations at CAA3 on the south side of the channel relative to CAA2 and CAA1.

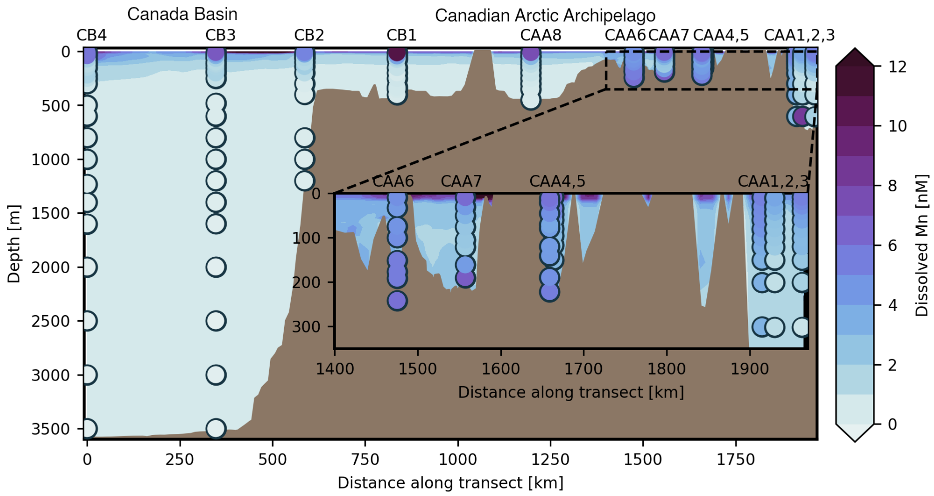

Figure 6. A transect of Mn concentrations from the Canada Basin through Parry Channel in the Canadian Arctic Archipelago to Baffin Bay (path shown in Fig. 5). Observations of dissolved Mn are shown within the circles, with the simulated concentrations for September, 2015 in the background. The inset expands on the Parry Channel region east of Barrow Sill.

The low and homogeneous background Mn concentrations are well represented in shallow (< 600 m) as well as deep stations (1000-3500 m depth). However, the background concentrations are underestimated at stations CAA1 and CAA6 in the central and eastern portions of Parry Channel (Fig. 5). At these stations, strong mixing results in constant, "vertical" Mn profiles (Hughes et al., 2018). During tuning, we saw that in these well-mixed regions, a locally higher sediment resuspension rate increased dMn concentrations from the bottom up to about 50 m depth where the surface stratification limits vertical mixing. At CAA1 and CAA6, although the high tidal speeds force some sediment resuspension to the west upstream in the model (Fig. 8b), it does not directly impact these stations. CAA1 also receives Baffin Bay water that recirculates into Lancaster Sound which is low in Mn content in the model. Nevertheless, sediment resuspension is well-represented in other regions such as station CAA9 in Penny Strait (sediment resuspension is the main source of Mn here; Fig. 8b), an area known for its strong tidal speeds and mixing (Hughes et al., 2018). At stations CAA2 and CAA7, on the south side of Parry Channel, observed Mn concentrations increase up to 10 nM near the ocean bottom. These peaks in the observations are attributed to sediment resuspension (Colombo et al., 2020), although the specific mechanism is unclear. The model does not reproduce these local extreme increases, which likely vary on much smaller spatial scales than our parameterizations can resolve. A small increase over the 40 m above the bottom is reproduced by the model at stations CAA5 and CAA7.

3.2 Importance of Sediment in Sea Ice

In the upper water column (above 50 m), the observed Mn concentrations are strongly variable and range from 2-11 nM. The "clean" sea ice experiment underestimates these concentrations by several nM (the mean of this experiment falls 3 nM below the 1:1 line), especially when observed concentrations exceed 6 nM (Fig. 7a). The reference run, which includes sediment in sea ice, represents observed concentrations reasonably well for concentrations below 6 nM and the mean falls close to the 1:1 line. In the eastern CAA, the reference run somewhat overestimates concentrations between 6-7 nM (especially nearest the surface), and underestimates the observed concentrations above 7 nM in the western CAA (stations CB1 and CAA8) which receive relatively direct outflow from the Arctic Ocean. In the upper bound river experiment, surface Mn concentrations are overestimated at most stations in the CAA, particularly in the eastern CAA, with a slight improvement at CAA8 in the western CAA (Fig. 7b). In the subsurface, CAA1, CAA2, and CAA5 in the eastern CAA are somewhat better represented. The Mn estimates for stations in the Canada Basin are unaffected by the addition of Mn originating from particulate matter in rivers.

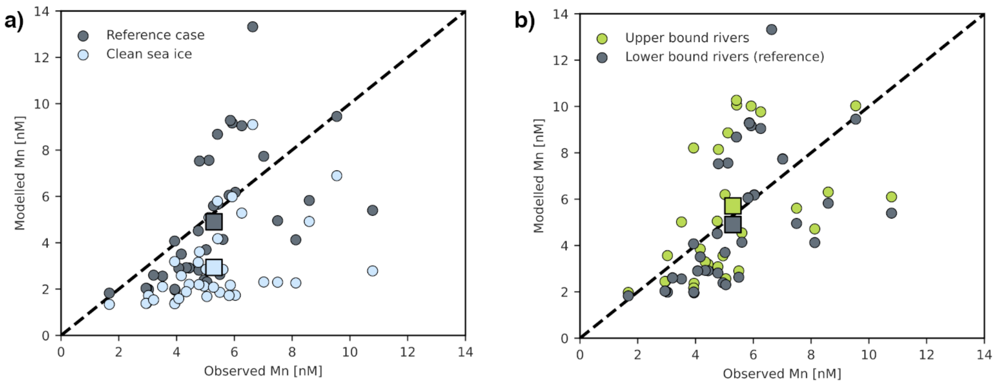

Figure 7. The nearest-depth modelled Mn concentrations compared with the observed concentrations at depths shallower than 50 m for all stations. Square markers indicate the averages of the experiments and observations. (a) The modelled Mn concentrations at the evaluation stations most closely resemble the observations in the reference experiment with sediment in sea ice compared to the “clean” sea ice experiment. Both of these experiments use the lower bound river estimate. (b) The lower and upper bound river experiments, which include sediment within the sea ice, indicate that a small additional contribution from riverine particulate matter content may be most representative.

In the near surface (around 10 m depth), observed concentrations range from 5-7 nM in the Canada Basin, up to 11 nM at CB1, while elsewhere in Parry Channel they are around 5 nM (Fig. 5 and 6). Within Parry Channel, the environment east of Barrow Sill is different from the regions west of Barrow Sill which share characteristics with the Canada Basin (Colombo et al., 2020). The model also displays this trend, however, the model overestimates the surface concentrations at some stations in eastern Parry Channel (CAA4-6), particularly in the upper bound river experiment. We expect substantial gradients in concentrations in the surface layer in the Arctic Ocean as a result of the strong stratification. The shallowest observations are collected at around 10 m below the surface, while the model surface estimate is at 0.5 m depth, so it is difficult to assess the uppermost modelled concentrations. However, the Mn-salinity relationship within the upper 50 m of the water column in the model is similar to the observations for the experiment with sediment in sea ice (Fig. S10). Without sediment in sea ice, the model underestimates the low-salinity Mn endmember.

While the model is limited in its representation of regions with strongly variable resuspension rates, it performs well within a range of environments: from deep regions in the Canada Basin to shallow areas in the CAA. The model is configured to ask questions about the drivers of Mn variability; it is important to keep in mind that our parameterizations are limited by the spatial and temporal resolution of available information, so small scale variations are unlikely to be captured by the model.

3.3 Contributions from External Sources of Mn

To assess the relative contributions of each of the external Mn sources, we calculated the annual contribution and flux from these model components in the reference experiment. We are most interested in the surface layer, so our estimate is for the upper 55 m of the water column. An estimate of the full water column differs by including the effects of resuspension in regions deeper than 55 m, thus increasing the importance of resuspension (Table S2). Estimates from the upper bound river experiment, which does not account for any removal of particulate or dissolved Mn in estuaries, are indicated in brackets. By calculating the Willmott skill score (Willmott, 1981), we estimate the optimal riverine suspended matter content for the model at the observed locations as $\beta = 0.05$ in Eqn. 3 (Willmott of 0.68). We did not include the contributions from (photo)reduction as a source of dMn in these calculations since it is part of the internal cycling of Mn. In order to identify regional differences, we separated the domain into the Canada Basin and the Canadian Arctic Archipelago (details in Fig. S3) and subdivided the CAA into western and eastern halves along 100°W. Overall, the Canada Basin is more isolated and receives a lower annual contribution of Mn than the CAA: 146 (162) versus 421 (547) μmol m^{-2} yr^{-1} (Table 2).

In our model, the dominant source of Mn in the Canada Basin is the release of sediment by sea ice melt (Table 2). This component accounts for 82 (74)% of the average yearly addition of Mn. The amount of melt that occurs fluctuates interannually, similar to sea ice extent changes observed with satellite data. Nevertheless, from 2002 to 2019, sea ice melt is consistently the largest contributor of Mn in our model in the Canada Basin.

Sediment resuspension contributes about 15 (13)% in the Canada Basin, mainly over the Beaufort shelf, and river discharge, predominantly from the Mackenzie River, contributes 3.6 (13)%. Atmospheric dust deposited onto the ocean surface, or released during sea ice melt, is not a significant source of Mn anywhere in the domain.

Table 2. The spatial average annual dissolved Mn contributed by external model source components to the upper 55 m of the water column (μmol m^{-2} yr^{-1}) in the reference experiment, averaged over the years 2002-2019, separated by region (Fig. S3). Sediment release by sea ice is the only component that varies significantly year-to-year. Estimates from the upper bound river contribution experiment are indicated in brackets.

	Canada Basin		Canadian Arctic Archipelago	
Component contribution	μmol m^{-2} yr^{-1}	%	μmol m^{-2} yr^{-1}	%
River discharge	5.2 (21)	3.6 (13)	15 (141)	3.5 (26)
Sediment resuspension	21	15 (13)	361	86 (66)
Sediment from sea ice	120	82 (74)	44	11 (8.1)
Dust released by sea ice	0.2	0.1	0.3	0.1
Direct dust deposition	0.0	0.0	0.0	0.0
Total	146 (162)	100	421 (547)	100

Table 3. Same as Table 2, but with the Canadian Arctic Archipelago (CAA) subdivided into western and eastern halves along 100°W (near Barrow Sill).

	Western CAA		Eastern CAA	
Component contribution	μmol m^{-2} yr^{-1}	%	μmol m^{-2} yr^{-1}	%
River discharge	5.8 (24)	1.8 (6.8)	22 (228)	4.4 (33)
Sediment resuspension	273	83 (79)	427	87 (61)
Sediment from sea ice	48	15 (14)	41	8.4 (5.9)
Dust released by sea ice	0.2	0.1	0.3	0.1
Direct dust deposition	0.0	0.0	0.0	0.0
Total	328 (345)	100	490 (696)	100

In the CAA, sediment resuspension contributes 86 (66)% of the annual external addition of Mn to the water column (Table 2). Sediment released by sea ice accounts for 11 (8.1)% of Mn; a combination of relatively "clean" sea ice with high melt rates. The importance of river contributions cover a broader range from 3.5 (26)% in the CAA, compared to 3.6 (13)% in the Canada Basin, however since these regions differ in total annual contributions, rivers contribute more dMn to the CAA overall. Although the Canada Basin receives runoff from the Mackenzie River, the CAA has many rivers of a range of sizes that drain into it, including glacial rivers with high Mn concentrations.

Within the CAA, there is a significant difference in dynamical regime west and east of the approximately 120 m deep Barrow Sill (Table 3; Hughes et al. (2017); Colombo et al. (2020); Q. Wang et al. (2012)). The overall contribution of Mn to the water column in the eastern CAA is 490 (696) μmol m^{-2} yr^{-1}, compared to 328 (345) μmol m^{-2} yr^{-1} in the western CAA. The main contributor to this difference is the 1.5 times stronger sediment resuspension in the eastern CAA. In addition, rivers contribute more strongly to the eastern CAA relative to the western CAA, 4.4 (33)% versus 1.8 (6.8)%, with a broad range in the estimate of their role in the eastern CAA. The eastern CAA receives contributions from the high Mn content glacial rivers that drain Greenland, Ellesmere Island, and Baffin Island.

Throughout our domain, Mn concentrations are highest in the summer months as a result of seasonally fluctuating components (Fig. 8a). Sea ice melt is largest in July, while the river runoff peak occurs during the freshet in May-June. Due to the large supply of dissolved Mn in the summer months and the increased solar flux, (photo)reduction and oxidation are stronger from July through September. For the month of September, we identified which model component is on average the dominant control of Mn for each horizontal grid cell over the full time series (Fig. 8b). Note that this figure shows where the model adds the contribution from a component; where the Mn ends up depends on the advection and diffusion of the tracer as well.

Within the Canada Basin and portions of the western CAA (the Amundsen Gulf and western Parry Channel), sea ice melt controls the simulated Mn concentrations (Fig. 8b). In the interior of the Beaufort Gyre region, far away from sources and with relatively "clean" sea ice, none of the components contribute significantly. Over the Beaufort Shelf, the Mackenzie River is a regionally important source of Mn; generally river runoff is a

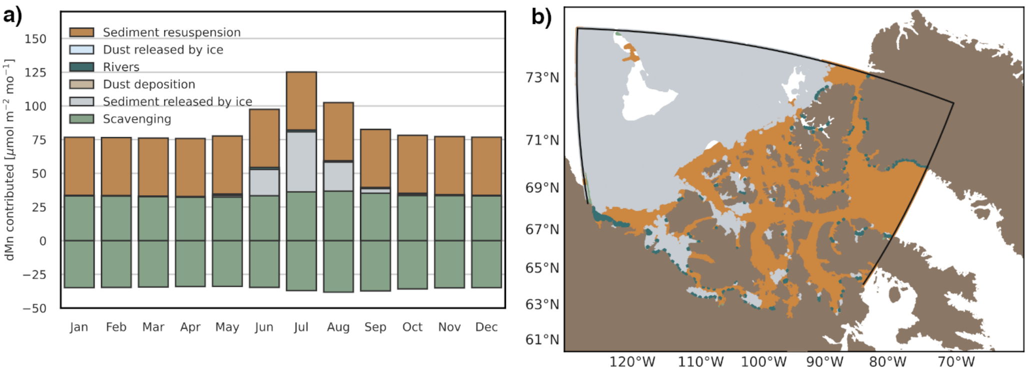

Figure 8. In the full water column, sediment released by sea ice dominates in the Canada Basin, while sediment resuspension is prevalent over shelf areas including the Canadian Arctic Archipelago. (a) Climatology of the seasonal cycle of Mn contributions for the full water column. The oxidation (removal) and reduction (addition) of Mn through scavenging are calculated as the average throughout the water column. Sediment resuspension is added at the bottom grid cell, while all other sources act directly on the ocean surface. Note that the contributions from dust deposition and release of dust from ice are too small to appear. (b) Most important Mn contributors to the water column in September based on climatology. At each grid cell, the color represents the most important model forcing component. The importance of scavenging is based on the average net combined effect of reduction and oxidation throughout the water column. Places where the net contributions are smaller than 0.5 μmol m^{-2} mo^{-1} are masked with white.

significant source at river mouths. In the shallower shelf regions, such as the Beaufort Shelf and the CAA, sediment resuspension is prevalent.

The magnitudes of annual Mn fluxes from sources in this Arctic Model (AM; Table 2) are comparable to those in the first global model of Mn by Van Hulten et al. (2017) (VH). In the global model, dust contributes 0-2 μmol m^{-2} yr^{-1} in the Arctic Ocean, whereas in AM it ranged from 0-1 μmol m^{-2} yr^{-1} (combining direct dust deposition from the atmosphere and indirect release from ice). AM riverine fluxes were 5.2 (21) μmol m^{-2} yr^{-1} in the Canada Basin and 15 (141) μmol m^{-2} yr^{-1} in the CAA; higher than the VH estimate of 0-2 μmol m^{-2} yr^{-1}. This range likely reflects a combination of the high Mn content of rivers in the Arctic used in this model (Colombo et al., 2019) and alternate treatment of rivers; VH assumes a relation between Fe and Mn content, while AM uses observations specific to the Arctic rivers and their catchment basins. In the global model, the flux of Mn from bottom sediments in the Arctic Ocean was 5-75 μmol m^{-2} yr^{-1}; AM has 21-361 μmol m^{-2} yr^{-1}. The difference in the upper limit of the range likely reflects the distinctive processes considered by the models: the global model considers sediment diffusion for the flux from sediments, whereas AM considers sediment resuspension because it is more important in the CAA (Colombo et al., 2020). It is also challenging to resolve the large continental shelf regions in the Canadian Arctic in a global model. Lastly, on a global scale, hydrothermal input of Mn at spreading ridges is important (Van Hulten et al., 2017), however the spreading ridges in the Arctic are far away from the AM domain, so that contribution is not included.

3.4 Simulated Surficial Mn During the Summer and the Polar Night

The most significant seasonal and interannual changes in Mn concentrations occur in the polar mixed layer, defined here as the upper 35 m of the water column. For the following characterizations of the simulated concentrations, we will focus on this layer. The upper few meters of the ocean have a strong gradient in Mn concentrations (simulated profile in Fig. S12). It is not possible to measure this layer with conventional methods from a large ship. As such, we exclude the surface 1 m in the results presented here (see Fig. S11 for the surface Mn field) to allow for more direct comparison with existing observations.

During the summer months, the surface Mn concentrations in the Canada Basin mirror the areas of strong sea ice melt (Fig. 9a). The highest Mn values are found along the outer edges of the Beaufort Gyre (up to 14 nM), while the interior has lower concentrations of Mn. The Beaufort Shelf does not receive a strong contribution of Mn from sea ice melt (Fig. 8b). The location of the areas with highest sea ice melt contributions in the Canada Basin shift from year-to-year with the position of the Beaufort Gyre.

Although rivers contribute only a few percent annually to Mn in the Canada Basin (Table. 2), over the continental shelf, plumes of high Mn concentrations extend along the coastline in the summer months (Fig. 9a). The plume from the Mackenzie River, the largest river in our domain, extends eastward along the shelf in July, 2015. In the southwestern CAA, high Mn concentrations are prevalent during the summer months in regions fed by continental rivers (Fig. 8b). Glacial river drainage is apparent in surface Mn concentrations in a number of coastal regions (Fig. 9a). A plume of runoff from Baffin Is-

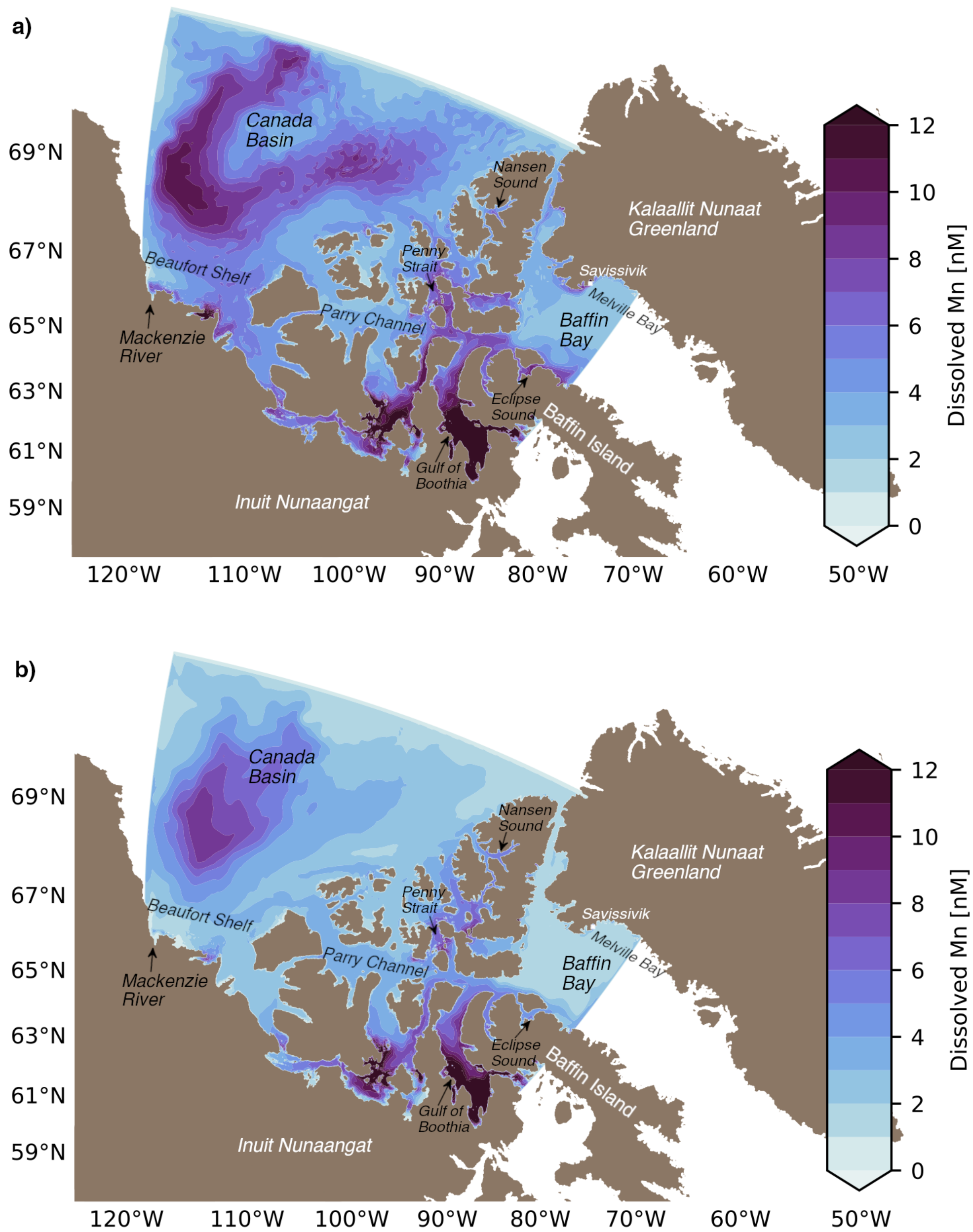

Figure 9. Simulated monthly average Mn concentrations in the Polar Mixed Layer. (a) July, 2015. In the summer, sea ice melt and sediment resuspension dominate the Mn concentrations in the Canada Basin and the Canadian Arctic Archipelago, while freshwater sources such as the Mackenzie River and Greenland meltwater are important regionally. (b) January, 2015. During the Polar night, simulated Mn concentrations are more homogeneous and low, however sediment resuspension continues to drive higher concentrations in the Gulf of Boothia and south-central CAA.

land extends from Eclipse Sound into Baffin Bay, where it is incorporated into the West Greenland Current. Along the coast of Greenland, high concentration Mn rivers drain the ice sheet and a number of plumes are visible. A notable plume is located near Savissivik into Melville Bay and extends along the shoreline. In the northern CAA, higher surface concentrations are a combination of the sea ice melt and glacial rivers (Fig. 8b). In particular, Nansen Sound receives large contributions from runoff from Ellesmere Island.

Mn concentrations exhibit strong spatial variability in the CAA (Fig. 9). In the western CAA, concentrations are low (2-6 nM) and homogeneous. Southern regions, including the Gulf of Boothia, have some of the highest concentrations (8-12+ nM) and flow into the Parry Channel east of Barrow Sill. In this section of central and eastern Parry Channel (and in Penny Strait), intermediate concentrations (6-9 nM) are present. In Lancaster Sound, the outflow from Parry Channel, with relatively high Mn concentrations, follows the southern half of the channel while lower concentration waters from Baffin Bay (1-4 nM) recirculate along the northern half of Lancaster Sound. Baffin Bay and the Nares Strait regions are characterized by lower surface concentrations.

During the Polar Night, fewer sources contribute Mn and there is less spatial contrast in surface concentrations (Fig. 9b). In the winter, surface concentrations range from 1-10 nM (excluding the Gulf of Boothia region), while in the summer they ranged up to 14 nM. Regions where Mn is most impacted by sediment resuspension (Fig. 8b), such as the Gulf of Boothia, still have high concentrations in the winter as this component does not vary seasonally. In the Canada Basin, a core of 4-10 nM concentrations is located towards the center of the Beaufort Gyre region, while during the summer months, the high concentrations are located around the outer edges (Fig. 9). The winter core forms from the advection of the summer Mn signal during the winter months when surface input in the Canada Basin is low, and from the reduction of oxidised Mn which was transported from regions with high summer dissolved Mn concentrations. The signature of this winter core reduces in the spring and early summer as the seasonal sea ice melt once again dominates the signal.

4 Discussion

In the Arctic Ocean, the maximum Mn concentrations occur near the surface in the polar mixed layer. These high concentrations are commonly attributed to freshwater sources such as river discharge and sea ice melt (Campbell & Yeats, 1982; Yeats & Westerlund, 1991; Middag et al., 2011b; Cid et al., 2012; Kondo et al., 2016; Colombo et al., 2020). However, the relative contributions from rivers and sea ice to this low-salinity maximum are not easily distinguished. In this paper, we present a regional model of Mn in the Canadian Arctic which incorporates river input and sediment release by sea ice, as well as atmospheric inputs, sediment resuspension, and scavenging. With these components, the model captures the spatial variability and magnitude of observed concentrations and we are able to use the model to assess the controls on Mn in the Arctic. With results from three Mn model experiments (reference, "clean" sea ice, and upper bound river), we identified the dominance of non-local sediment released by sea ice in the Canada Basin, while rivers had a more regional importance. These findings suggest that future changes to sea ice transport across the Arctic Ocean may have a significant impact on the supply of Mn and other nutrients to the Canada Basin and downstream to the CAA. Within the CAA, the dynamical differences between the western and eastern CAA translated into distinctive mean Mn concentrations and component contribution patterns with more influence from rivers and sediment resuspension.

4.1 Ice-rafted Sediments are the Predominant Source of Mn in the Canada Basin

With our model, we found that 82 (74)% of Mn in the Canada Basin (the main estimate is from the reference experiment with the upper bound river estimate in brackets) is supplied by sediment from sea ice and 11 (8.1)% in the CAA (Table 2). Sediments released by sea ice melt dominate the Mn concentrations in the polar mixed layer during the summer months (Fig. 9a), while in the winter, sea ice blocks the direct surface input of Mn and a relatively lower, more homogeneous distribution results (Fig. 9b). These results indicate that sediment transport and release by sea ice is the main source of Mn (and likely other similar nutrients) within the Canada Basin, and plays a role within the CAA as well. The sea ice in the interior of the Canada Basin originates from the Siberian shelf regions and traverses the Arctic Ocean via the transpolar drift. The sea ice spends several years in transit, during which it undergoes freeze-thaw cycles and loses sediment.

In the Canada Basin, the highest Mn concentrations (and relatively younger ice) are found along the outer edges of the Beaufort Gyre, while older ice transported to the interior of the Gyre by convergence has lower Mn concentrations (Fig. 9a). Sea ice is also formed in the Beaufort Shelf region, however this ice is transported towards Siberia and does not directly impact the Mn concentrations in the Canada Basin.

Mn sources from the land-ocean interface, such as rivers and sediments, were more important in the CAA than in the Canada Basin, and dynamical differences between the western and eastern CAA translated into distinctive Mn concentrations and component contribution patterns. This separation in dynamics is bounded by the ≈120 m deep Barrow Sill and has been noted in several studies (Hughes et al., 2017; Colombo et al., 2020). In the western CAA, surface concentrations range from 3-6 nM (Fig. 9) and Mn component contributions share characteristics with the Canada Basin: similar overall river contributions, some influence from sediments in sea ice, and weaker contributions from sediment resuspension than in the eastern CAA (Table 3). In contrast, in the eastern CAA, Mn concentrations are high (6-9 nM; Fig. 9) and dominated by sediment resuspension associated with strong tidal speeds and river discharge plays a more important role. The estimate of the component contributions is most sensitive in the eastern CAA: the importance of rivers ranges from 4.4% in the reference experiment up to a maximum of 33% in the upper bound river experiment. Rivers are prevalent in the eastern CAA and many of these drain glaciated regions associated with high suspended particulate matter and dissolved Mn. As a result, rivers have the potential to play an important role for Mn in the eastern CAA. However, the available information for river input and estuarine removal limits our ability to constrain the most likely river contribution. Based on the model versus observation surface comparisons (Fig. 7), the upper bound river experiment overestimates the contribution of rivers because it does not consider removal in estuaries, but the lower bound river experiment underestimates it. The most realistic value is somewhere in between. The uncertainties associated with these estimates highlight the need for studies looking at the estuarine cycling in the CAA.

Besides sea ice melt, Pacific water inflow from the Bering Strait and river runoff (Eurasian runoff and North American runoff) contribute freshwater to the Arctic Ocean (Proshutinsky et al., 2019; Krishfield et al., 2014) and could contribute Mn to the surface maximum. The central Canada Basin contains significant amounts of meteoric water and sea ice melt (Guay et al., 2009) which feed its freshening (Yamamoto-Kawai et al., 2009). Several studies have looked into the composition of this water. Fichot et al. (2013) did not identify much river runoff in the central basin and Kelly et al. (2019) found that the freshwater contribution from Siberian rivers has decreased since 1997 as a result of the mainly anticyclonic atmospheric circulation pattern over the Canada Basin. Similarly, model trajectories of floats released from Siberian rivers since 1985 do not generally reach the Canada Basin by 2007 (Proshutinsky et al., 2019). In our reference and upper bound river simulations, rivers contribute only 3.6 (13)% to the total budget of Mn in the Canada Basin and 3.5 (26)% in the CAA (Table 2). However, freshwater sources such as the Mackenzie River on the Beaufort shelf and glacial melt off the coast of Greenland (Fig. 9) do dominate areas nearby coastlines. The supply of relatively fresh Pacific Water from Bering Strait to the Canada Basin is also affected by the atmospheric circulation in the Canada Basin (Kelly et al., 2019) and floats released from Bering Strait since 2000 do not enter the central Canada Basin by 2012 (Proshutinsky et al., 2019). Thus, inputs outside of our domain that originate from Siberian runoff and Pacific water are unlikely to significantly contribute to the freshwater-associated surface Mn maximum in the Canada Basin. It is important to note that our simulated profiles (Fig. 5) do not capture the subtle increase in Mn concentrations associated with the winter Bering Sea Water around 100-200 m depth in the Canada Basin. This limitation is likely because our western boundary condition does not fully capture the higher concentrations of Mn found in the Alaskan Coastal Current and in waters from the Chukchi Shelf. This difference mainly affects the Beaufort Shelf and as mentioned the winter Bering Sea Water layer in the Canada Basin.

In order to assess whether we overestimated the sediment content of sea ice, we performed an experiment with “clean” sea ice. In the “clean” ice experiment, the surface Mn concentrations are underestimated by 3 nmol L^{-1} or about 30-50% in the Canada Basin relative to observations (Fig. 7a). If we assume that all of the missing Mn comes from sediment and that Mn added at the surface mixes down to the turbocline, we miss a source that supplies 10-160 grams of sediment per squared meter to the surface ocean across the Canada Basin (range based on model turbocline depths in 2015). The magnitude of this component is similar to the average sediment load measured in sea ice cores (Reimnitz et al., 1993; Stierle & Eicken, 2002; Eicken et al., 2005). Rivers would be unable to contribute the total amount missing since it must occur over a large area and since the upper bound river experiment shows that additional contributions from rivers do not significantly affect the Canada Basin or the overall surface representation (Fig. 7b). In the "clean" sea ice experiment, the freshwater endmember of Mn is also underestimated (Fig. S10). The Mn-salinity relationship in the Canada Basin and the CAA is more accurately represented in the experiment with sediment contained in sea ice and the regional differences are also reproduced.

Our results demonstrate that the long range transport of sediments by sea ice from the Siberian shelves is an important source of Mn in the Canada Basin and the Canadian Arctic Archipelago. These findings provide support for the sea ice trace metal transport mechanism proposed by Measures (1999). Measures (1999) found that the highest Al and Fe concentrations in the central Arctic Ocean coincided with areas with high concentrations of ice-rafted sediments, instead of river input, and so they hypothesized that transport of ice rafted sediments and the subsequent seasonal melt supplies reactive elements to the surface Arctic Ocean. However, their data set did not allow the quantification of annual fluxes of material to the central Arctic Ocean and so they were unable to quantify the exact contribution of this component to the observed trace metal concentrations.

4.2 Declining Long Range Sea Ice Transport Could Reduce the Canada Basin and Canadian Arctic Archipelago Nutrient Supply

Based on the importance of non-local sediments transported by sea ice (particularly from the Siberian shelves), the distributions of trace metals, nutrients, and their biogeochemical cycles in the Arctic basins are likely to be significantly impacted by climate change associated reductions in sea ice. Rising oceanic and atmospheric temperatures delay the freeze-up period and induce earlier melt of sea ice (Stroeve et al., 2012; Stroeve & Notz, 2018). In addition, in the relatively "quiet" dynamics of the Arctic Ocean, increased mixing may bring warmer Atlantic water (or Pacific Water; Kodaira et al. (2020)) to the surface and further increase sea ice melt (D'Asaro & Morison, 1992; Liang & Losch, 2018). These factors may significantly reduce the amount of first-year ice that survives in the Kara Sea, East Siberian sea, and western Laptev Sea (Krumpen et al., 2019).

Investigations of long range transport by the transpolar ice drift indicate an increase in exchange of ice-rafted material between regions, associated with faster ice drift from thinning ice cover (Spreen et al., 2011; Kwok et al., 2013; Kipp et al., 2018). However, Krumpen et al. (2019) found that summer ice extents in the marginal ice zones have been low enough over the past few years, that most of the ice exported from shelves melts before it enters the transpolar drift. Only ice formed in polynyas between October and January was advected far enough to survive the following summer melt season, suggesting a reduction in the transport of matter towards the central Arctic Ocean and Fram Strait.

In our study, we saw a steady increase in the Mn content of the Canada Basin polar mixed layer from 2002-2019 (Fig. 10), and the primary source of this Mn is sea ice melt (correlation R-squared of 0.57). Note that in our model experiments, we do not account for changes in sea ice supply regions, but focus only on sea ice melt. The addition of Mn by melt in our model mirrors satellite observations of sea ice loss in the Beaufort Sea (Fig. 10; correlation R-squared of 0.54). So, the short term increase in sea ice melt may increase the Mn content of the Canada Basin. However, the long term reduction in supply of sediment rich sea ice from the Siberian shelves via the transpolar drift and the reduction in total sea ice volume would result in a decreased supply of Mn. Whereas in the short term, there may be an increase in nutrients supplied by sea ice into the Canada Basin through increased sea ice exchange and melt, in the long run, we expect a decrease in supply and a subsequent decline in the surface maximum of Mn in the Canada Basin. Confounding this is the likely increase in transport of riverine and shelf-derived trace elements in the ocean by the transpolar drift as a result of an intensification of the Arctic hydrological cycle and permafrost degradation (Charette et al., 2020).

A reduction in nutrient supply to the Canada Basin may also have an impact downstream in Baffin Bay. With our experiments, we calculated the transport of Mn through Parry Channel and the contribution of sediment released by sea ice melt and rivers to this transport (see Text S2 for details). About 45% of the net Mn transported into Parry Channel from the Canada Basin is contributed by sediments from sea ice and 7% by rivers (Fig. S4 and S5). Rivers contribute 4% to the Mn transported from Parry Channel into Baffin Bay and sea ice contributes around 18%. The reduction in the contribution of these components does not indicate loss in the CAA; it reflects the additional contributions from sediment resuspension from the CAA shelf environment. The sea ice contribution in the water column is significant downstream, however, it is important to note that the sea ice transport in the CAA in the ocean-ice model is stronger than observed due to the lack of a land-fast ice parameterization (Grivault et al., 2018). As a result, we may overestimate the sea ice transport and thus melt in Parry Channel, particularly for the out-

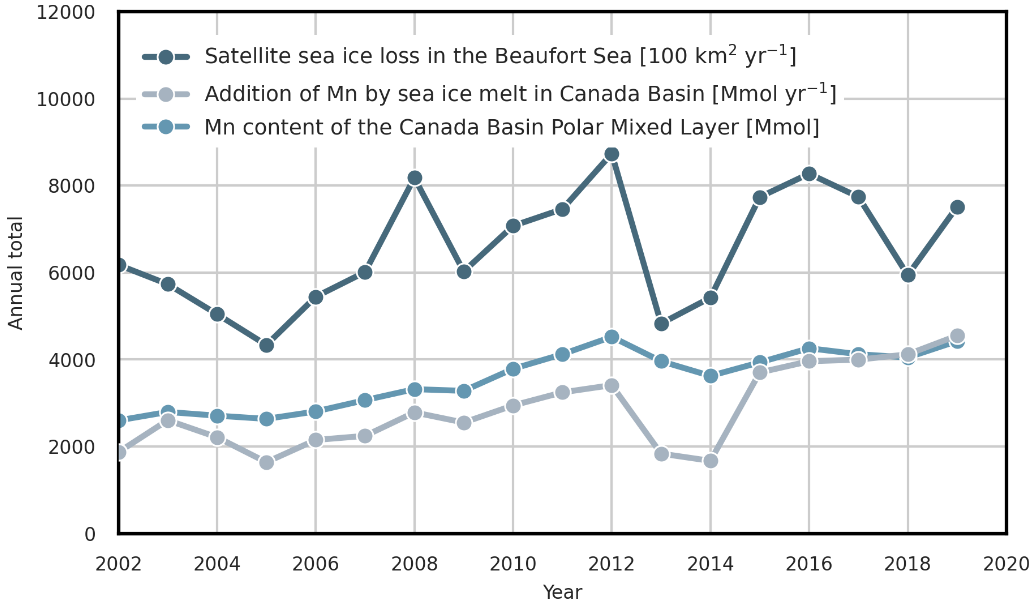

Figure 10. Interannual variations in sea ice melt contribute strongly to Mn supply to the Canada Basin. Conversely, surface Mn concentration changes in the Canada Basin can be used as an indicator of the volume of sediments released by sea ice melt. The sea ice loss is calculated from regional monthly sea ice extent changes measured by the Defense Meteorological Satellite Program series of passive microwave remote sensing instruments (Fetterer et al., 2017). The Mn added by external sources to the Canada Basin is calculated from outputs of the regional Mn model presented in this study.

flow from Parry Channel into Baffin Bay. There are also further factors contributing Mn within the CAA which confound this finding. The acceleration of the hydrological cycle and permafrost thaw may increase the contributions of riverine Mn to the CAA; our experiments do not take these changes into account. On the other hand, sea ice melt is associated with an increase in stratification which may reduce the depth up to which resuspended sediment can mix, reducing the Mn supplied into the upper water column (and productive areas) by sediment resuspension in the CAA. However, reduced sea ice cover is also associated with increased wind-driven mixing.

Our findings for Mn in the Arctic have implications for nutrients which share similar sources. In the Arctic Ocean, iron (Fe) behaves similarly to Mn, although Fe is less soluble than Mn and oxidizes more rapidly (Landing and Bruland (1987); Colombo et al. (2020); for a comprehensive discussion, read Jensen et al. (2020)). Fe is an essential micronutrient and in some regions of the ocean, such as the Southern Ocean, parts of the North Atlantic, and the Pacific Northwest, it limits primary productivity (Martin & Gordon, 1988; Hawkings et al., 2014; Tagliabue et al., 2017). Generally, iron is not growth limiting in the Arctic (S. Wang et al., 2014), but there is evidence that Fe is limited in some specific regions: on the outer shelf and shelf break in the Bering Sea (Aguilar-Islas et al., 2008), as well as in the Barents Sea and Nansen Basin (Rijkenberg et al., 2018). Past studies have indicated that sea ice contributes to the flux of Fe into the ocean (Measures, 1999; Lannuzel et al., 2007; Aguilar-Islas et al., 2008; Kanna et al., 2020). Based on the expected changes to the Mn cycle and supply with sea ice melt over the next decades, the supply of Fe to the Canada Basin may be reduced as well. Meanwhile, the increase in simulated Mn content in the Canada Basin from 2002-2019 due to sea ice melt may also have supplied nutrients such as Fe and drive some of the observed increased Arctic Ocean primary production (Lewis et al., 2020). Changes to Fe availability impact the community composition and the timing of the spring phytoplankton bloom (Aguilar-Islas et al., 2008), which in turn has consequences for biological productivity, Arctic ecosystems, and the carbon cycle.

4.3 Limitations of Results

The findings in this study are limited by the parameterizations for scavenging, sediment in sea ice, sediment resuspension, and river runoff. Overall, the model is best constrained for summer months, the southern CAA, and the Canada Basin due to the availability of observations. Scavenging rates are important throughout the water column and are most likely to affect our results in coastal regions. We assumed steady state to estimate the adsorption and desorption rates from observations; this assumption is least likely to hold in coastal regions and near the surface where scavenging rates are both important and variable. For the sediment released by sea ice, we did not account for variations in transport of sediment (and its origin) across the Arctic Ocean over the course of the time series. Sea ice drift patterns vary interannually, and so could the source regions for sediment transported to the Canada Basin by sea ice. The sediment content would more accurately be represented as a time dependent variable. The total Mn content in the Canada Basin would increase (decrease) with a higher (lower) sediment content in sea ice, while sediment in sea ice would be more (less) important overall. However, observed sediment sea ice loads range several orders of magnitude by location sampled and properties of the ice, and these fluctuations make it challenging to quantify annual changes in overall sediment content and path travelled. Similarly, sediment resuspension varies interannually and seasonally and may be better represented as a time dependent variable. We do not take into account the contributions from breaking of internal waves, storm generated currents, and surface waves on sediment resuspension. As a result, we likely underestimate sediment resuspension contributions in some areas, particularly during the summer ice-free period. Our treatment of rivers was simplistic and did not account for the complexity of transformations that occur in the estuarine zone. Our results indicate a lower and upper bound of the riverine contributions, however we are unable to indicate what the actual contribution is. We also did not account for the projected seasonal ranges in riverine Mn concentrations with discharge (Colombo et al., 2019); the river discharge varies seasonally, but the characteristic Mn concentrations of the rivers are constant. This approximation could underestimate the riverine contributions during the spring freshet in coastal areas. The regions most likely to be impacted by these limitations are within the northern CAA and Greenland coast, where glacial rivers are most important.

While the numbers presented here should be taken as an estimate of magnitude rather than as exact values, the key results are robust to the uncertainties described above. The only way we were able to close the Mn budget (particularly in the Canada Basin) was by incorporating the sediment in sea ice component. Similarly, the only way to represent the higher concentrations of Mn found in the lower water column at some stations in the CAA was through the sediment resuspension term. Overall, while the model is limited in its representation of these processes, it provides a platform to ask questions about the drivers of Mn variability and to perform larger scale estimates of the processes that contribute Mn to the Arctic Ocean. Improvements to the estimates of sediment content in sea ice from, for example, satellite products would strengthen future predictions, while the model accuracy would be improved by more comprehensive estimates of the scavenging and sediment resuspension rates. Observations of Mn along a transect from an estuary into the ocean would help constrain the riverine contributions.

5 Conclusions

New trace metal datasets collected in the Arctic Ocean as part of the Canadian GEOTRACES program have provided an essential base for studying biogeochemical cycling in this unique region. Using in situ observations from Colombo et al. (2020), we developed the first model of Mn in the Canadian Arctic Archipelago and the Canada Basin. With three experiments from 2002-2019, we looked at (1) the drivers of Mn distributions in the CAA and the Canada Basin and (2) implications of future sea ice transport changes on the biogeochemical cycles of nutrients in the Arctic Ocean.

(1) While sediment transport by sea ice is identified as important in the Arctic Ocean (Measures, 1999; Eicken et al., 2005), this mechanism is commonly considered less significant for Mn than riverine input. However, without the contribution from sediment in sea ice to Mn, we were unable to accurately represent the Mn concentrations in the Canada Basin with our model. Sediments transported in sea ice by the transpolar drift account for up to 82% of the total annual Mn added in the Canada Basin and up to 15% in the western CAA, driving Mn surface maxima. These results support the hypothesis that "ice-rafted sediment may be an important transport mechanism for supplying reactive trace elements," proposed by Measures (1999). Rivers are certainly locally important, but contribute only 3.6 (13)% annually in the Canada Basin. Within the CAA, our estimates for river contributions ranged from 3.5% up to 26% in the upper bound river experiment. This broad range is the result of the limited information available regarding estuarine cycling in the Arctic. A clear divide is present in the CAA: west of Barrow Sill, the mean concentrations are lower and the behaviour of Mn is more similar to the Canada Basin, while in the eastern CAA, sediments resuspended by high tidal speeds, as well as many glacial rivers drive higher Mn concentrations.

(2) Sea ice transport via the transpolar drift is interrupted by Arctic warming (Krumpen et al., 2019) and the decline in this long range transport could reduce the Canada Basin and the CAA nutrient supply. These changes not only impact the Arctic, but also sub-arctic seas, with 18% of the Mn transported from Parry Channel into Baffin Bay added by sea ice melt. Mn behaves similarly to Fe in the Arctic Ocean and both of these nutrients support phytoplankton growth. The importance of sea ice for nutrient supply to the photic zone in the Canada Basin, as well as downstream, is concerning given the recent changes in the Arctic Ocean sea ice regime (reduced summer minimum ice extent, ice thinning, reduction in multi-year ice extent, and altered drift paths). There are many competing factors that will contribute to changes in the biogeochemical cycles; combined model-observation studies are highly valuable to understand the individual contribution of these factors.

Acronyms

CAA Canadian Arctic Archipelago

NEMO Nucleus for European Modelling of the Ocean

ANHA12 Arctic and Northern Hemispheric Atlantic 1/12 degree

LIM2 Louvain-la-Neuve version 2

TOP Tracers in the Ocean Paradigm

TVD Total Variance Dissipation scheme

CESM Community Earth System Model

CAM-Chem Community Atmosphere Model with Chemistry

Acknowledgments

We thank Marco van Hulten for openly sharing his model code and results, Jacqui-Lee Epstein for extracting the tidal speeds for the sediment resuspension parameterization, and Genevieve Parton for helpful discussions regarding sediment resuspension. This work was funded by the National Sciences and Engineering Council (NSERC) Climate Change and Atmospheric Research Grant: GEOTRACES (RGPCC 433848-12) and VITALS (RGPCC 433898), an NSERC Discovery Grant (RGPIN-2016-03865) to SEA, and by the University of British Columbia through a four year fellowship to BR. Computing resources were provided by Compute Canada (RRG 2648 RAC 2019, RRG 2969 RAC 2020, RRG

1541 RAC 2021). The model configuration, code, results, and analysis code are archived on FRDR at https://doi.org/10.20383/102.0388. Analysis code is also available via Github at https://github.com/brogalla/Mn-sea-ice-paper.

References

Aguilar-Islas, A. M., Rember, R. D., Mordy, C. W., & Wu, J. (2008). Sea ice-derived dissolved iron and its potential influence on the spring algal bloom in the Bering Sea. *Geophys. Res. Lett.*, *35*(24). doi: 10.1029/2008GL035736

Bacon, S., Marshall, A., Holliday, N. P., Aksenov, Y., & Dye, S. R. (2014). Seasonal variability of the East Greenland Coastal Current. *J. Geophys. Res.-Ocean.*, *119*(6), 3967–3987. doi: 10.1002/2013JC009279

Balzer, W. (1982). On the distribution of iron and manganese at the sediment/water interface: Thermodynamic versus kinetic control. *Geochem. Cosmochim. Acta*, *46*(7), 1153–1161. doi: 10.1016/0016-7037(82)90001-1

Bamber, J., Van Den Broeke, M., Ettema, J., Lenaerts, J., & Rignot, E. (2012). Recent large increases in freshwater fluxes from Greenland into the North Atlantic. *Geophys. Res. Lett.*, *39*(19).

Bouillon, S., Morales Maqueda, M. A., Legat, V., & Fichefet, T. (2009). An elastic-viscous-plastic sea ice model formulated on Arakawa B and C grids. *Ocean Model.*, *27*(3-4), 174–184. doi: 10.1016/j.ocemod.2009.01.004

Brand, L. E., Sunda, W. G., & Guillard, R. R. L. (1983). Limitation of marine phytoplankton reproductive rates by zinc, manganese, and iron. *Limnol. Oceanogr.*, *28*(6), 1182–1198. doi: 10.4319/lo.1983.28.6.1182

Brown, K. A., Williams, W. J., Carmack, E. C., Fiske, G., François, R., McLennan, D., & Peucker-Ehrenbrink, B. (2020). Geochemistry of small Canadian Arctic rivers with diverse geological and hydrological settings. *J. Geophys. Res.-Biogeosciences*, *125*(1). doi: 10.1029/2019JG005414

Bruland, K. W., Donat, J. R., & Hutchins, D. A. (1991). Interactive influences of bioactive trace metals on biological production in oceanic waters. *Limnol. Oceanogr.*, *36*(8), 1555–1577. doi: 10.4319/lo.1991.36.8.1555

Bruland, K. W., Orians, K. J., & Cowen, J. P. (1994). Reactive trace metals in the stratified central North Pacific. *Geochem. Cosmochim. Acta*, *58*(15), 3171–3182. doi: 10.1016/0016-7037(94)90044-2

Campbell, J. A., & Yeats, P. A. (1982). The distribution of manganese, iron, nickel, copper and cadmium in the waters of Baffin Bay and the Canadian Arctic Archipelago. *Oceanol. Acta*, *5*(2), 161–168.

Carrère, L., & Lyard, F. (2003). Modeling the barotropic response of the global ocean to atmospheric wind and pressure forcing-comparisons with observations. *Geophys. Res. Lett.*, *30*(6).

Charette, M. A., Kipp, L. E., Jensen, L. T., Dabrowski, J. S., Whitmore, L. M., Fitzsimmons, J. N., ... others (2020). The Transpolar Drift as a source of riverine and shelf-derived trace elements to the central Arctic Ocean. *J. Geophys. Res.-Ocean.*, *125*(5). doi: 10.1029/2019jc015920

Charette, M. A., Lam, P. J., Lohan, M. C., Kwon, E. Y., Hatje, V., Jeandel, C., ... Garcia-Orellana, J. (2016). Coastal ocean and shelf-sea biogeochemical cycling of trace elements and isotopes: lessons learned from GEOTRACES. *Philos. Trans. Roy. Soc. A*, *374*(2081), 20160076. doi: 10.1098/rsta.2016.0076

Chelton, D. B., de Szoeke, R. A., Schlax, M. G., El Naggar, K., & Siwertz, N. (1998). Geographical variability of the first baroclinic Rossby radius of deformation. *J. Phys. Oceangr.*, *28*(3), 433–460. doi: 10.1175/1520-0485(1998)028%3C0433:GVOTFB%3E2.0.CO;2

Cid, A. P., Nakatsuka, S., & Sohrin, Y. (2012). Stoichiometry among bioactive trace metals in the Chukchi and Beaufort Seas. *J. Oceanogr.*, *68*(6), 985–1001. doi: 10.1007/s10872-012-0150-8

Colombo, M., Brown, K. A., De Vera, J., Bergquist, B. A., & Orians, K. J. (2019). Trace metal geochemistry of remote rivers in the Canadian Arctic Archipelago. *Chem. Geol.*, *525*, 479–491. doi: 10.1016/j.chemgeo.2019.08.006

Colombo, M., Jackson, S. L., Cullen, J. T., & Orians, K. J. (2020). Dissolved iron and manganese in the Canadian Arctic Ocean: on the biogeochemical processes controlling their distributions. *Geochem. Cosmochim. Acta*, *277*, 150–174. doi: 10.1016/j.gca.2020.03.012

Dai, A., Qian, T., Trenberth, K. E., & Milliman, J. D. (2009). Changes in continental freshwater discharge from 1948 to 2004. *J. Climate*, *22*(10), 2773–2792. doi: 10.1175/2008JCLI2592.1

Damm, E., Bauch, D., Krumpen, T., Rabe, B., Korhonen, M., Vinogradova, E., & Uhlig, C. (2018). The Transpolar Drift conveys methane from the

Siberian Shelf to the central Arctic Ocean. *Sci. Rep.*, *8*(1), 1–10. doi: 10.1038/s41598-018-22801-z

Darby, D. A., Myers, W. B., Jakobsson, M., & Rigor, I. (2011). Modern dirty sea ice characteristics and sources: The role of anchor ice. *J. Geophys. Res.-Ocean.*, *116*(9). doi: 10.1029/2010JC006675

D'Asaro, E. A., & Morison, J. H. (1992). Internal waves and mixing in the Arctic Ocean. *Deep Sea Res. Pt. I*, *39*(2), S459–S484. doi: 10.1016/S0198-0149(06)80016-6

Dethleff, D., & Kuhlmann, G. (2009). Entrainment of fine-grained surface deposits into new ice in the southwestern Kara Sea, Siberian Arctic. *Cont. Shelf Res.*, *29*(4), 691–701. doi: 10.1016/j.csr.2008.11.009

Dethleff, D., & Kuhlmann, G. (2010). Fram Strait sea-ice sediment provinces based on silt and clay compositions identify Siberian Kara and Laptev seas as main source regions. *Polar Sci.*, *29*(3). doi: 10.3402/polar.v29i3.6070

Dethleff, D., Rachold, V., Tintelnot, M., & Antonow, M. (2000). Sea-ice transport of riverine particles from the Laptev Sea to Fram Strait based on clay mineral studies. *Intl. J. Earth Sci.*, *89*(3), 496–502. doi: 10.1007/s005310000109

Drinkwater, K. F., & Harding, G. C. (2001). Effects of the Hudson Strait outflow on the biology of the Labrador Shelf. *Can. J. Fish. Aquat. Sci.*, *58*(1), 171–184. doi: 10.1139/f00-210

Eicken, H., Gradinger, R., Gaylord, A., Mahoney, A., Rigor, I., & Melling, H. (2005). Sediment transport by sea ice in the Chukchi and Beaufort Seas: Increasing importance due to changing ice conditions? *Deep Sea Res. Pt. II*, *52*, 3281–3302. doi: 10.1016/j.dsr2.2005.10.006

Eicken, H., Kolatschek, J., Freitag, J., Lindemann, F., Kassens, H., & Dmitrenko, I. (2000). A key source area and constraints on entrainment for basin-scale sediment transport by Arctic sea ice. *Geophys. Res. Lett.*, *27*(13), 1919–1922. doi: 10.1029/1999GL011132

Eicken, H., Reimnitz, E., Alexandrov, V., Martin, T., Kassens, H., & Viehoff, T. (1997). Sea-ice processes in the Laptev Sea and their importance for sediment export. *Cont. Shelf Res.*, *17*(2), 205–233. doi: 10.1016/S0278-4343(96)00024-6

Epstein, J.-L. (2018). *The impact of internal tide mixing parameterizations in* *an eddy-permitting model of the Arctic Ocean* (Master's thesis, University of British Columbia). doi: 10.14288/1.0365809

Evans, L. K., & Nishioka, J. (2018). Quantitative analysis of Fe, Mn and Cd from sea ice and seawater in the Chukchi Sea, Arctic Ocean. *Polar Sci.*, *17*, 50–58. doi: 10.1016/j.polar.2018.07.002

Fetterer, F., Knowles, K., Meier, W. N., Savoie, M., & Windnagel, A. K. (2017). Updated daily: Sea ice index, version 3. Boulder, Colorado USA. *NSIDC: National Snow and Ice Data Center*. doi: 10.7265/N5K072F8

Fichefet, T., & Maqueda, M. A. M. (1997). Sensitivity of a global sea ice model to the treatment of ice thermodynamics and dynamics. *J. Geophys. Res.-Ocean.*, *102*(C6), 12609–12646. doi: 10.1029/97JC00480

Fichot, C. G., Kaiser, K., Hooker, S. B., Amon, R. M., Babin, M., Bélanger, S., ... Benner, R. (2013). Pan-Arctic distributions of continental runoff in the Arctic Ocean. *Sci. Rep.*, *3*(1), 1–6. doi: 10.1038/srep01053

Fishwick, M. P., Ussher, S. J., Sedwick, P. N., Lohan, M. C., Worsfold, P. J., Buck, K. N., & Church, T. M. (2018). Impact of surface ocean conditions and aerosol provenance on the dissolution of aerosol manganese, cobalt, nickel and lead in seawater. *Mar. Chem.*, *198*, 28–43. doi: 10.1016/J.MARCHEM.2017.11.003

Gent, P. R., Willebrand, J., McDougall, T. J., & McWilliams, J. C. (1995). Parameterizing eddy-induced tracer transport in ocean circulation models. *J. Phys. Oceangr.*, *25*(4), 463–474. doi: 10.1175/1520-0485(1995)025%3C0463:PEITTI%3E2.0.CO;2

Granskog, M. A., Kaartokallio, H., & Shirasawa, K. (2003). Nutrient status of Baltic Sea ice: Evidence for control by snow-ice formation, ice permeability, and ice algae. *J. Geophys. Res.-Ocean.*, *108*(C8). doi: 10.1029/2002jc001386

Greene, C. H., & Pershing, A. J. (2007). Climate drives sea change. *Science*, *315*(5815), 1084–1085. doi: 10.1126/science.1136495

Grivault, N., Hu, X., & Myers, P. G. (2018). Impact of the surface stress on the volume and freshwater transport through the Canadian Arctic Archipelago from a high-resolution numerical simulation. *J. Geophys. Res.-Ocean.*, *123*(12), 9038–9060. doi: 10.1029/2018JC013984

Guay, C. K. H., McLaughlin, F. A., & Yamamoto-Kawai, M. (2009). Differentiating fluvial components of upper Canada Basin waters on the basis of measurements of dissolved barium combined with other physical and chemical tracers. *J. Geophys. Res.-Ocean.*, *114*(C1). doi: 10.1029/2008JC005099

Hawkings, J. R., Wadham, J. L., Tranter, M., Raiswell, R., Benning, L. G., Statham, P. J., . . . Telling, J. (2014). Ice sheets as a significant source of highly reactive nanoparticulate iron to the oceans. *Nat. Commun.*, *5*(1), 1–8. doi: 10.1038/ncomms4929

Hayashida, H., Christian, J. R., Holdsworth, A. M., Hu, X., Monahan, A. H., Mortenson, E., . . . Steiner, N. S. (2019). CSIB v1 (Canadian Sea-ice Biogeochemistry): a sea-ice biogeochemical model for the NEMO community ocean modelling framework. *Geosci. Model Dev.*, *12*(5), 1965-1990.

Hölemann, J., Wegener, A., & Schirmacher, M. (1999). Dissolved and particulate major and trace elements in newly formed ice from the Laptev Sea (Transdrift III, October 1995). In *Land-ocean systems in the Siberian Arctic* (pp. 101–111). Springer Berlin Heidelberg. doi: 10.1007/978-3-642-60134-7_11

Holland, M. M., Bailey, D. A., Briegleb, B. P., Light, B., & Hunke, E. (2012). Improved sea ice shortwave radiation physics in CCSM4: The impact of melt ponds and aerosols on Arctic sea ice. *J. Climate*, *25*(5), 1413–1430. doi: 10.1175/JCLI-D-11-00078.1

Hu, X., Myers, P. G., & Lu, Y. (2019). Pacific water pathway in the Arctic Ocean and Beaufort Gyre in two simulations with different horizontal resolutions. *J. Geophys. Res.-Ocean.*, *124*(8), 6414–6432.

Hu, X., Sun, J., Chan, T. O., & Myers, P. G. (2018). Thermodynamic and dynamic ice thickness contributions in the Canadian Arctic Archipelago in NEMO-LIM2 numerical simulations. *Cryosphere*, *12*, 1233–1247. doi: 10.5194/tc-12-1233-2018

Hughes, K. G., Klymak, J. M., Hu, X., & Myers, P. G. (2017). Water mass modification and mixing rates in a 1/12 simulation of the Canadian Arctic Archipelago. *J. Geophys. Res.-Ocean.*, *122*, 803–820. doi: 10.1002/2016JC012235

Hughes, K. G., Klymak, J. M., Williams, W. J., & Melling, H. (2018). Tidally modulated internal hydraulic flow and energetics in the central Canadian Arctic Archipelago. *J. Geophys. Res.-Ocean.*, *123*(8), 5210–5229. doi: 10.1029/2018JC013770

Hunter, J. D. (2007). Matplotlib: A 2d graphics environment. *Comput. Sci. Eng.*, *9*(3), 90–95.

Jakobsson, M. (2002). Hypsometry and volume of the Arctic Ocean and its constituent seas. *Geochem. Geophys. Geosystems*, *3*(5), 1–18. doi: 10.1029/2001GC000302

Jensen, L. T., Morton, P., Twining, B. S., Heller, M. I., Hatta, M., Measures, C. I., … Fitzsimmons, J. N. (2020). A comparison of marine Fe and Mn cycling: U.S. GEOTRACES GN01 Western Arctic case study. *Geochem. Cosmochim. Acta*. doi: 10.1016/j.gca.2020.08.006

Johnson, K. S., Coale, K. H., Berelson, W. M., & Michael Gordon, R. (1996). On the formation of the manganese maximum in the oxygen minimum. *Geochem. Cosmochim. Acta*, *60*(8), 1291–1299. doi: 10.1016/0016-7037(96)00005-1

Kanna, N., Lannuzel, D., van der Merwe, P., & Nishioka, J. (2020). Size fractionation and bioavailability of iron released from melting sea ice in a subpolar marginal sea. *Mar. Chem.*, *221*, 103774. doi: 10.1016/j.marchem.2020.103774

Kay, J. E., Deser, C., Phillips, A., Mai, A., Hannay, C., Strand, G., … Vertenstein, M. (2015). The community earth system model (CESM) large ensemble project : A community resource for studying climate change in the presence of internal climate variability. *B. Am. Meteorol. Soc.*, *96*(8), 1333–1349. doi: 10.1175/BAMS-D-13-00255.1

Kelly, S. J., Proshutinsky, A., Popova, E. K., Aksenov, Y. K., & Yool, A. (2019). On the origin of water masses in the Beaufort Gyre. *J. Geophys. Res.-Ocean.*, *124*(7), 4696–4709. doi: 10.1029/2019JC015022

Kempema, E. W., Reimnitz, E., & Barnes, P. (1989). Sea ice sediment entrainment and rafting in the Arctic. *J. Sediment. Petrol.*, *59*(2), 308–317.

Kipp, L. E., Charette, M. A., Moore, W. S., Henderson, P. B., & Rigor, I. G. (2018). Increased fluxes of shelf-derived materials to the central Arctic Ocean. *Sci. Advances*, *4*(1). doi: 10.1126/sciadv.aao1302

Klinkhammer, G. P., & Bender, M. L. (1980). The distribution of manganese in the Pacific Ocean. *Earth Planet Sc. Lett.*, *46*(3), 361–384. doi: 10.1016/0012-821X(80)90051-5

Kluyver, T., Ragan-Kelley, B., Pérez, F., Granger, B., Bussonnier, M., Frederic, J., … others (2016). *Jupyter notebooks – a publishing format for reproducible* *computational workflows* (F. Loizides & B. Schmidt, Eds.). IOS Press.

Kodaira, T., Waseda, T., Nose, T., & Inoue, J. (2020). Record high Pacific Arctic seawater temperatures and delayed sea ice advance in response to episodic atmospheric blocking. *Sci. Rep.*, *10*(1), 1–12.

Kondo, Y., Obata, H., Hioki, N., Ooki, A., Nishino, S., Kikuchi, T., & Kuma, K. (2016). Transport of trace metals (Mn, Fe, Ni, Zn and Cd) in the western Arctic Ocean (Chukchi Sea and Canada Basin) in late summer 2012. *Deep Sea Res. Pt. I*, *116*, 236–252. doi: 10.1016/J.DSR.2016.08.010

Krachler, M., Zheng, J., Fisher, D., & Shotyk, W. (2005). Analytical procedures for improved trace element detection limits in polar ice from Arctic Canada using ICP-SMS. *Anal. Chim. Acta*, *530*(2), 291–298. doi: 10.1016/j.aca.2004.09.024

Krishfield, R. A., Proshutinsky, A., Tateyama, K., Williams, W. J., Carmack, E. C., McLaughlin, F. A., & Timmermans, M. L. (2014). Deterioration of perennial sea ice in the Beaufort Gyre from 2003 to 2012 and its impact on the oceanic freshwater cycle. *J. Geophys. Res.-Ocean.*, *119*(2), 1271–1305. doi: 10.1002/2013JC008999

Krumpen, T., Belter, H. J., Boetius, A., Damm, E., Haas, C., Hendricks, S., ... Stein, R. (2019). Arctic warming interrupts the Transpolar Drift and affects long-range transport of sea ice and ice-rafted matter. *Sci. Rep.*, *9*(1), 1–9. doi: 10.1038/s41598-019-41456-y

Kwok, R., Spreen, G., & Pang, S. (2013). Arctic sea ice circulation and drift speed: Decadal trends and ocean currents. *J. Geophys. Res.-Ocean.*, *118*(5), 2408–2425. doi: 10.1002/jgrc.20191

Landing, W. M., & Bruland, K. W. (1987). The contrasting biogeochemistry of iron and manganese in the Pacific Ocean. *Geochem. Cosmochim. Acta*, *51*(1), 29–43. doi: 10.1016/0016-7037(87)90004-4

Lange, M., & van Sebille, E. (2017). Parcels v0.9: Prototyping a Lagrangian ocean analysis framework for the petascale age. *Geosci. Model Dev.*, *10*(11), 4175–4186. doi: 10.5194/gmd-10-4175-2017

Lannuzel, D., Schoemann, V., de Jong, J., & Tison, J.-L. (2007). Distribution and biogeochemical behaviour of iron in the East Antarctic sea ice. *Mar. Chem.*, *106*(1-2), 18–32. doi: 10.1016/J.MARCHEM.2006.06.010

Lavelle, J. W., Cowen, J. P., & Massoth, G. J. (1992). A model for the deposition of hydrothermal manganese near ridge crests. *J. Geophys. Res.*, *97*(C5), 7413. doi: 10.1029/92JC00406

Lévy, M., Estublier, A., & Madec, G. (2001). Choice of an advection scheme for biogeochemical models. *Geophys. Res. Lett.*, *28*(19), 3725–3728. doi: 10.1029/2001GL012947

Lewis, K. M., van Dijken, G. L., & Arrigo, K. R. (2020). Changes in phytoplankton concentration now drive increased Arctic Ocean primary production. *Science*, *369*(6500), 198–202. doi: 10.1126/science.aay8380

Li, J. (2017). *Particulate trace metals and iron availability to phytoplankton in a changing Arctic Ocean* (Master's thesis, University of British Columbia). doi: 10.14288/1.0348666

Liang, X., & Losch, M. (2018). On the effects of increased vertical mixing on the Arctic Ocean and sea ice. *J. Geophys. Res.-Ocean.*, *123*(12). doi: 10.1029/2018JC014303

Macdonald, R. W., & Gobeil, C. (2012). Manganese sources and sinks in the Arctic Ocean with reference to periodic enrichments in basin sediments. *Aquat. Geochem.*, *18*(6), 565–591. doi: 10.1007/s10498-011-9149-9

Madec, G. (2008). NEMO ocean engine. *Note du Pôle de modélisation, Institut Pierre-Simon Laplace*, *27*(1288-1619). Retrieved from `https://www.nemo-ocean.eu/wp-content/uploads/NEMO_book.pdf`

Martin, J. H., & Gordon, R. M. (1988). Northeast Pacific iron distributions in relation to phytoplankton productivity. *Deep Sea Res. Pt. I*, *35*(2), 177–196. doi: 10.1016/0198-0149(88)90035-0

Masina, S., Storto, A., Ferry, N., Valdivieso, M., Haines, K., Balmaseda, M., ... Parent, L. (2017). An ensemble of eddy-permitting global ocean reanalyses from the MyOcean project. *Clim. Dynam.*, *49*(3), 813–841. doi: 10.1007/s00382-015-2728-5

Measures, C. I. (1999). The role of entrained sediments in sea ice in the distribution of aluminium and iron in the surface waters of the Arctic Ocean. *Mar. Chem.*, *68*, 59–70. doi: 10.1016/S0304-4203(99)00065-1

Middag, R., de Baar, H. J. W., Laan, P., Cai, P. H., & van Ooijen, J. C. (2011a). Dissolved manganese in the Atlantic sector of the Southern Ocean. *Deep Sea Res. Pt. II*, *58*(25-26), 2661–2677. doi: 10.1016/J.DSR2.2010.10.043

Middag, R., de Baar, H. J. W., Laan, P., & Klunder, M. B. (2011b). Fluvial and hydrothermal input of manganese into the Arctic Ocean. *Geochem. Cosmochim. Acta*, *75*(9), 2393–2408. doi: 10.1016/J.GCA.2011.02.011

Newton, R., Pfirman, S., Tremblay, B., & DeRepentigny, P. (2017). Increasing transnational sea-ice exchange in a changing Arctic Ocean. *Earths Future*, *5*(6), 633–647. doi: 10.1002/2016EF000500

Nürnberg, D., Wollenburg, I., Dethleff, D., Eicken, H., Kassens, H., Letzig, T., & Reimnitz, E. (1994). Sediments in Arctic sea ice: Implications for entrainment, transport and release. *Mar. Geol.*, *119*, 185–214. doi: 10.1016/0025-3227(94)90181-3

O'Brien, M. C., Macdonald, R. W., Melling, H., & Iseki, K. (2006). Particle fluxes and geochemistry on the Canadian Beaufort Shelf: Implications for sediment transport and deposition. *Cont. Shelf Res.*, *26*(1), 41–81. doi: 10.1016/J.CSR.2005.09.007

Oliphant, T. E. (2006). *A guide to numpy* (Vol. 1). Trelgol Publishing USA.

Pedregosa, F., Varoquaux, G., Gramfort, A., Michel, V., Thirion, B., Grisel, O., ... Duchesnay, E. (2011). Scikit-learn: Machine learning in Python. *J. Mach.*, *12*, 2825–2830.

Peeken, I., Primpke, S., Beyer, B., Gütermann, J., Katlein, C., Krumpen, T., ... Gerdts, G. (2018). Arctic sea ice is an important temporal sink and means of transport for microplastic. *Nat. Commun.*, *9*(1), 1–12. doi: 10.1038/s41467-018-03825-5

Pfirman, S. L., Eicken, H., Bauch, D., & Weeks, W. (1995). The potential transport of pollutants by Arctic sea ice. *Sci. Total Environ.*, *159*(2-3), 129–146. doi: 10.1016/0048-9697(95)04174-Y

Proshutinsky, A., Krishfield, R., Toole, J. M., Timmermans, M. L., Williams, W., Zimmermann, S., ... Zhao, J. (2019). Analysis of the Beaufort Gyre freshwater content in 2003–2018. *J. Geophys. Res.-Ocean.*, *124*(12), 9658–9689. doi: 10.1029/2019JC015281

Reimnitz, E., Mccormick, M., Mcdougall, K., & Brouwers, E. (1993). Sediment export by ice rafting from a coastal polynya. *Arct. Antarct. Alp. Res.*, *25*(2), 83–98. doi: 10.1080/00040851.1993.12002988

Rijkenberg, M. J. A., Slagter, H. A., van der Loeff, M., van Ooijen, J., & Gerringa,

L. J. A. (2018). Dissolved Fe in the deep and upper Arctic Ocean with a focus on Fe limitation in the Nansen Basin. *Front. Mar. Sci.*, *5*, 88. doi: 10.3389/fmars.2018.00088

Smith, G. C., Roy, F., Mann, P., Dupont, F., Brasnett, B., Lemieux, J.-F., ... Bélair, S. (2014). A new atmospheric dataset for forcing ice-ocean models: Evaluation of reforecasts using the Canadian global deterministic prediction system. *Q. J. R. Meteorol. Soc.*, *140*(680), 881–894. doi: 10.1002/qj.2194

Spreen, G., Kwok, R., & Menemenlis, D. (2011). Trends in Arctic sea ice drift and role of wind forcing: 1992-2009. *Geophys. Res. Lett.*, *38*(19). doi: 10.1029/2011GL048970

Stierle, A. P., & Eicken, H. (2002). Sediment inclusions in Alaskan coastal sea ice: Spatial distribution, interannual variability, and entrainment requirements. *Arct. Antarct. Alp. Res.*, *34*(4), 465–476. doi: 10.1080/15230430.2002.12003518

Stroeve, J. C., & Notz, D. (2018). Changing state of Arctic sea ice across all seasons. *Environ. Res. Lett.*, *13*(10). doi: 10.1088/1748-9326/aade56

Stroeve, J. C., Serreze, M. C., Holland, M. M., Kay, J. E., Malanik, J., & Barrett, A. P. (2012). The Arctic's rapidly shrinking sea ice cover: A research synthesis. *Clim. Change*, *110*(3-4), 1005–1027. doi: 10.1007/s10584-011-0101-1

Sunda, W. G., & Huntsman, S. A. (1994). Photoreduction of manganese oxides in seawater. *Mar. Chem.*, *46*(1-2), 133–152. doi: 10.1016/0304-4203(94)90051-5

Tagliabue, A., Bowie, A. R., Boyd, P. W., Buck, K. N., Johnson, K. S., & Saito, M. A. (2017). The integral role of iron in ocean biogeochemistry. *Nature*, *543*(7643), 51–59. doi: 10.1038/nature21058

The Pandas development team. (2020). Pandas-dev/pandas: Pandas. *Zenodo*, *21*, 1–9.

Thyng, K. M., Greene, C. A., Hetland, R. D., Zimmerle, H. M., & DiMarco, S. F. (2016). True colors of oceanography: Guidelines for effective and accurate colormap selection. *Oceanogr.*, *29*(3), 9–13.

Tilmes, S., Lamarque, J. F., Emmons, L. K., Kinnison, D. E., Marsh, D., Garcia, R. R., ... Blake, N. (2016). Representation of the Community Earth System Model (CESM1) CAM4-chem within the Chemistry-Climate Model Initiative (CCMI). *Geosci. Model Dev.*, *9*(5), 1853–1890. doi: 10.5194/gmd-9-1853-2016

Tovar-Sánchez, A., Duarte, C. M., Alonso, J. C., Lacorte, S., Tauler, R., & Galbán-Malagón, C. (2010). Impacts of metals and nutrients released from melting multiyear Arctic sea ice. *J. Geophys. Res.*, *115*(C7), C07003. doi: 10.1029/2009JC005685

Tucker, W. B., Gow, A. J., Meese, D. A., Bosworth, H. W., & Reimnitz, E. (1999). Physical characteristics of summer sea ice across the Arctic Ocean. *J. Geophys. Res.-Ocean.*, *104*(C1), 1489–1504. doi: 10.1029/98jc02607

Van Hulten, M., Middag, R., Dutay, J.-C., De Baar, H., Roy-Barman, M., Gehlen, M., ... Sterl, A. (2017). Manganese in the west Atlantic Ocean in the context of the first global ocean circulation model of manganese. *Biogeosciences*, *14*, 1123–1152. doi: 10.5194/bg-14-1123-2017

Virtanen, P., Gommers, R., Oliphant, T. E., Haberland, M., Reddy, T., Cournapeau, D., ... others (2020). Scipy 1.0: fundamental algorithms for scientific computing in python. *Nature methods*, *17*(3), 261–272.

Wang, Q., Myers, P. G., Hu, X., & Bush, A. B. G. (2012). Flow constraints on pathways through the Canadian Arctic Archipelago. *Atmos.-Ocean*, *50*(3), 373–385.

Wang, S., Bailey, D., Lindsay, K., Moore, J. K., & Holland, M. (2014). Impact of sea ice on the marine iron cycle and phytoplankton productivity. *Biogeosciences*, *11*(17), 4713–4731. doi: 10.5194/bg-11-4713-2014

Waskom, M., & the Seaborn development team. (2020). *Seaborn.* Zenodo. doi: 10.5281/zenodo.592845

Wedepohl, H. K. (1995). The composition of the continental crust. *Geochem. Cosmochim. Acta*, *59*(7), 1217–1232. doi: 10.1016/0016-7037(95)00038-2

Willmott, C. J. (1981). On the validation of models. *Phys. Geogr.*, *2*(2), 184–194.

Yamamoto-Kawai, M., McLaughlin, F. A., Carmack, E. C., Nishino, S., Shimada, K., & Kurita, N. (2009). Surface freshening of the Canada Basin, 2003–2007: River runoff versus sea ice meltwater. *J. Geophys. Res.*, *114*(C1), C00A05. doi: 10.1029/2008JC005000

Yeats, P. A., & Westerlund, S. (1991). Trace metal distributions at an Arctic Ocean ice island. *Mar. Chem.*, *33*(3), 261–277. doi: 10.1016/0304-4203(91)90071-4

Zalesak, S. T. (1979). Fully multidimensional flux-corrected transport algorithms for fluids. *J. Comput. Phys.*, *31*(3), 335–362. doi: 10.1016/0021-9991(79)90051-2